Ore Geology Reviews 77 (2016) 43–56

Contents lists available at ScienceDirect

Ore Geology Reviews

journal homepage: www.elsevier.com/locate/oregeorev

In-situ LA–ICP–MS U–Pb geochronology and trace elements analysis of polygenetic titanite from the giant Beiya gold–polymetallic deposit in Yunnan Province, Southwest China

Yu Fu [a,b,d], Xiaoming Sun [a,b,c,d,*], Haoyang Zhou [b,c], Hai Lin [a,b], Tianjian Yang [b,c]

[a] School of Marine Sciences, Sun Yat-sen University, Guangzhou 510006, China
[b] Guangdong Provincial Key Laboratory of Marine Resources and Coastal Engineering, Guangzhou 510275, China
[c] School of Earth Science and Geological Engineering, Sun Yat-sen University, Guangzhou 510275, China
[d] South China Sea Bio-Resource Exploitation and Utilization Collaborative Innovation Center, Guangzhou 510006, China

ARTICLE INFO

Article history:
Received 20 November 2015
Received in revised form 1 February 2016
Accepted 3 February 2016
Available online 12 February 2016

Keywords:
Titanite
U–Pb dating
Trace elements
Beiya
Gold deposit
SW China

ABSTRACT

The Beiya gold–polymetallic deposit, located in the middle of the Jinshajiang–Ailaoshan alkaline porphyry metallogenic belt, is one of the largest gold deposits in China. The mineralization mainly occurs in skarn along the intrusive contacts between the alkaline porphyries and Middle Triassic limestone. In this paper, we present U–Pb age as well as major and trace element geochemistry of titanite from the Beiya deposit, and distinguish the titanite into a magmatic- and a hydrothermal suite. Our study indicates that the titanite from the ore-related porphyry and from the mineralized skarn is texturally and geochemically very different. The euhedral, envelope-shaped titanite from the ore-related porphyry has lower FeO, F, HFSEs, Nb/Ta and Lu/Hf, together with higher TiO_2 and Th/U than the subhedral titanite from the mineralized skarn. The titanite from the porphyry also displays higher LREE/HREE and more subtle negative Eu anomaly than its mineralized skarn counterpart. This suggests a magmatic- and a hydrothermal origin for, respectively, the titanite from the ore-related porphyry and from the mineralized skarn. In-situ magmatic titanite U–Pb dating has yielded an Eocene age of 36.0 ± 5.9 Ma, consistent with the porphyry zircon U–Pb age (36.07 ± 0.43 Ma) obtained in previous studies. Hydrothermal titanite has yielded a weighted average $^{206}Pb/^{238}U$ age of 33.1 ± 1.0 Ma (MSWD = 2.0), which represents the age of the retrograde skarn alteration and the maximum age for the gold mineralization. Together with the previous molybdenite Re–Os age, we have further constrained the Beiya gold–polymetallic metallogeny to 33.1–34.1 Ma. The mineralization age is slightly younger than the porphyry emplacement, indicating that the Beiya metallogeny was likely to be a post-magmatic hydrothermal product of the Himalayan orogenic event. The REE characteristics of hydrothermal titanite also reveal that the ore forming fluids may have been derived from a highly oxidized magma.

1. Introduction

Titanite ($CaTiSiO_5$) is a common accessory mineral in magmatic and metamorphic rocks, as well as in hydrothermal alteration products such as skarn. Titanite typically accommodates significant amount of Rare Earth Elements (REEs) and High Field Strength Elements (HFSEs) (Tiepolo et al., 2002; Gao et al., 2012; Deng et al., 2015a), and the titanite generated from different origins exhibit distinct trace element geochemistry (Storey et al., 2007; Horie et al., 2008; Smith et al., 2009; Xie et al., 2010; Gao et al., 2012; Che et al., 2013; Guo et al., 2014; Ismail et al., 2014; Cao et al., 2015; Xu et al., 2015). Therefore, trace element geochemistry of titanite can serve as an indicator of its formation environment (Mazdab, 2009; Che et al., 2013; Ismail et al., 2014; Xu et al., 2015). Zirconium content of titanite is temperature- and pressure sensitive, and thus can be used as an important thermobarometer (Hayden et al., 2008). Furthermore, titanite Nd isotope can shed light on its petrogenesis (Gregory et al., 2009; Sun et al., 2010; Cao et al., 2015). Like zircon, titanite can accommodate considerable U and Th (with high closure temperatures of up to 700 °C), but it is more susceptible to high temperature hydrothermal alteration than zircon. This makes titanite suitable for recording complex magmatic, metamorphic and hydrothermal processes (Frost et al., 2000; Tiepolo et al., 2002; Deng et al., 2015a). Thus, titanite U–Pb dating has been widely used on magmatic, hydrothermal and metamorphic events dating in recent years (Corfu and Grunsky, 1987; Pan et al., 1993; Corfu et al., 1994;

* Corresponding author at: School of Earth Sciences and Geological Engineering and School of Marine Sciences, Sun Yat-sen University, Guangzhou 510006, China.
E-mail address: eessxm@mail.sysu.edu.cn (X. Sun).

http://dx.doi.org/10.1016/j.oregeorev.2016.02.001
0169-1368/

Esssex and Gromet, 2000; Aleinikoff et al., 2002; Storey et al., 2007; Chiaradia et al., 2009; Smith et al., 2009; Li et al., 2010; Sun et al., 2010; Kohn and Corrie, 2011; Fallourd et al., 2014; Sepahi et al., 2014; Bonamici et al., 2015; Chelle-Michou et al., 2015; Deng et al., 2015a). Nevertheless, the issue that titanite commonly incorporates non-negligible common Pb makes it difficult to yield a concordant age (Frost et al., 2000). Besides, owing to a lack of universal high quality titanite standard for in-situ laser ablation–inductively coupled plasma–mass spectrometry (LA–ICP–MS) dating, many laboratories use zircon as an external standard and some use raster scan mode instead of spot mode to reduce the matrix effect during laser ablation. The analytical mode, however, may have little effect to the age obtained (Sun et al., 2012), and a number of studies have shown that accurate and precise titanite U–Pb ages can be obtained by using zircon standards, such as 91500 and GJ-1 (Storey et al., 2007; Li et al., 2010; Sun et al., 2010; Fallourd et al., 2014; Deng et al., 2015a).

The Beiya gold–polymetallic deposit, located in the middle of the Jinshajiang–Ailaoshan alkaline porphyry metallogenic belt, is the largest gold deposit in the region (reserve: 304 t gold) and contains significant amounts of Fe, Cu, Ag, Pb and Zn. Given the close genetic relationship between the Himalayan (Cenezoic) alkaline porphyries and the Beiya ore deposit (Hou et al., 2004; Guo et al., 2005; Xu et al., 2006a, 2006b, 2007a; Xue et al., 2008; He et al., 2012, 2013; Deng et al., 2015b; Liu et al., 2015), understanding the age and genesis of the metallogeny and alkaline porphyries at Beiya is crucial not only for the Beiya mineral district, but also for the entire Jinshajiang–Ailaoshan metallogenic belt. Precise and accurate age constraints on the magmatic–hydrothermal events in porphyry systems are fundamental to understand how such deposits are formed and how the magmatism and mineralization are related (Chiaradia et al., 2013). Previous studies have mainly focused on dating the Beiya alkaline porphyries (ca. 33–37 Ma; Xu et al., 2007b; Xiao et al., 2009; Lu et al., 2012, 2013a, 2013b; Deng et al., 2015b; Liu et al., 2015), whereas direct and accurate dating of the mineralization was very limited (Fu et al., 2015; He et al., 2015). In this study, we report the occurrence of two titanite types at Beiya, i.e., magmatic- and hydrothermal titanite. In-situ geochemical analyses of these two titanite types have been conducted using EPMA and LA–ICP–MS to characterize the Beiya titanite and to elucidate its genesis. We also present new titanite U–Pb ages and compare them with the published zircon U–Pb and molybdenite Re–Os ages, in order to better constrain the magmatic–hydrothermal evolution of the Beiya mineralization.

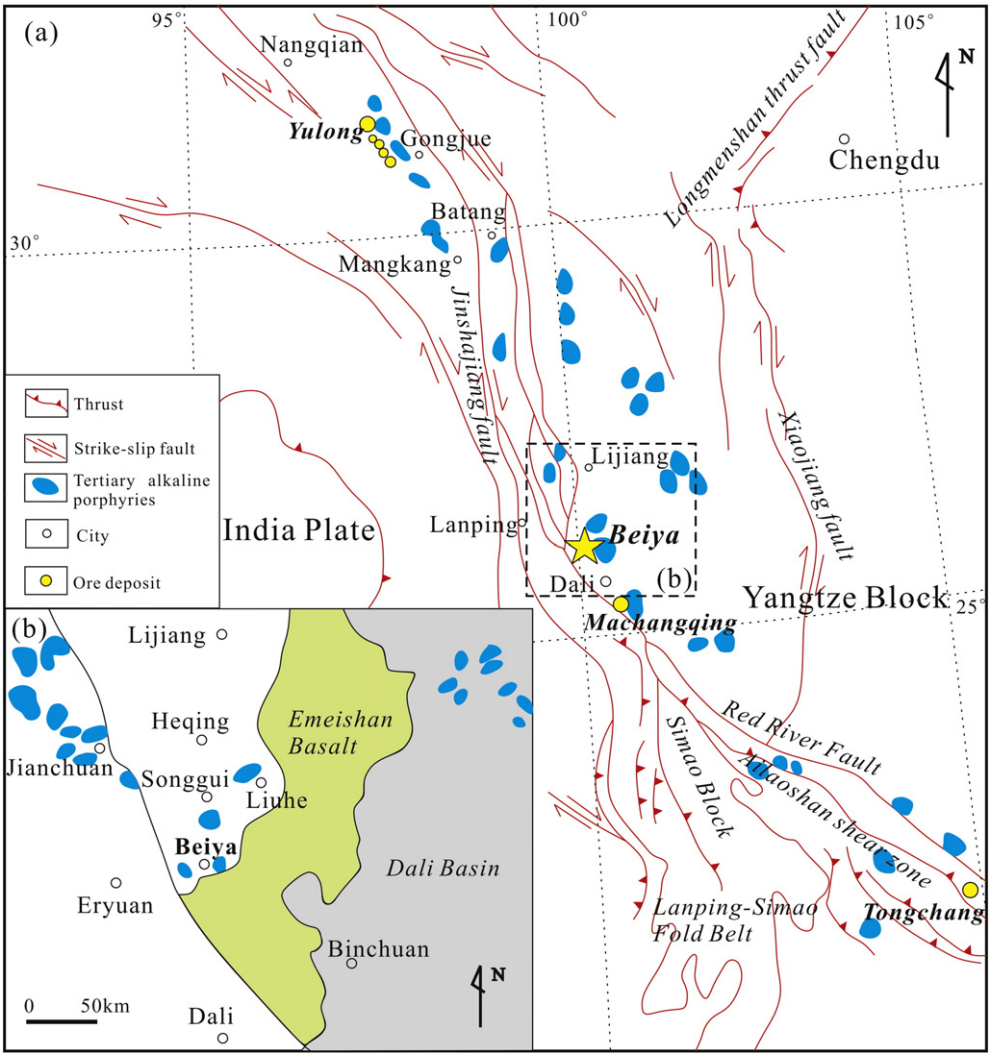

Fig. 1. Tectonic setting of the Beiya area.
Revised after Wang et al. (2001) and Hou et al. (2004).

2. Geological setting and ore geology

2.1. Geological setting

The Beiya gold–polymetallic deposit (90 km north of Dali in western Yunnan, SW China) is geologically situated to east of the Jinshajiang suture, the western boundary of the Yangtze Plate (Fig. 1). The deposit has an estimated reserves of 125.6 million tons (Mt) gold (average grade: 2.42 g/t), 138 Mt iron (average grade: 33.3 wt.%), 122.9 Mt copper (average grade: 0.48 wt.%), along with considerable amounts of lead, zinc and silver. The Beiya deposit includes six ore segments, namely the Weiganpo, Bijiashan and Guogaishan ore segments in the east and the Wandongshan, Hongnitang and Jingouba ore segments in the west (Fig. 2a). Among these ore segments, Wandongshan is the major one and contains the majority of the resources. The exposed strata at Beiya mainly comprise the Lower Triassic Qingtianbao Formation (175–350 m thick), containing arkose, hornfelsed greywacke and sandstone with basaltic volcaniclastic rocks; the Middle Triassic Beiya Formation contains dolomitic limestone, ferruginous limestone, bioclastic limestone and argillaceous limestone (ca. 138–531 m thick, the main ore-bearing rock); and Quaternary sedimentary rocks. The Upper Permian Emeishan Formation basalt occurs in the southeastern part of the Beiya peripheral area. Cenezoic Himalayan alkaline porphyries are abundant, but relatively minor at Beiya. These alkaline rocks include (quartz) syenite porphyry, biotite–K-feldspar porphyry and quartz–albite porphyry (Xu et al., 2006b, 2007b; Xue et al., 2008), and are closely related to the mineralization spatially and temporally. Several faults with different orientation exist in the orefield, among which the N-S-striking faults are dominant, such as Maanshan fault. It belongs to the secondary fault system of the Jinshajiang–Honghe strike-slip fault (Li et al., 2016). This fault passed through the western area of orefield and the derived secondary fracture controlled the porphyries and orebodies of Wandongshan and Hongnitang ore segments in the Beiya deposit.

2.2. Ore deposit geology

Skarn is the main mineralization type in the Beiya deposit and the skarn ore bodies mostly occur in the contact zones between porphyry intrusions and the carbonate host rocks of the Beiya Formation, which were strictly controlled by the structure and alteration of contact zones. The ore body KT52 around the Wandongshan porphyry is the largest skarn ore body (Fig. 2b) with proven reserves of 87.2 Mt gold (mean grade: 2.35 g/t), along with 90.27 Mt of iron ore (average grade: 34 wt.% Fe), 111.8 Mt of copper ore (average grade: 0.34 wt.% Cu) (Li et al., 2016). The skarn metallogeny comprises four major stages: (1) prograde skarn, (2) retrograde skarn, (3) quartz–sulfide, and (4) supergene stages. Prograde skarn minerals are mainly anhydrous, such as garnet and diopside (Fig. 3a–c), whereas mineral assemblages in retrograde stage are predominantly hydrous, including epidote-group mineral, biotite, chlorite, titanite and K-feldspar (Fig. 3d, e). Magnetite mineralization mainly occurred during the late retrograde stage. The quartz–sulfide stage is featured by the mineralization of pyrite, chalcopyrite, pyrrhotite and molybdenite (Fig. 3f), and is associated with gold mineralization. The supergene stage is characterized by secondary enriched oxide ore bodies with gold-bearing hematite and limonite, which are regarded as the products of weathering and leaching of the primary sulfides. At Beiya, gold mainly occurs as native gold and electrum, which typically occur in cracks or as vein-filling in pyrite, limonite, quartz and other minerals; it can also be wrapped in sulfides, such as pyrite. The compositions of the Beiya skarn minerals suggest a typical oxidized skarn system (He et al., 2015). Studies of fluid inclusions indicate the characteristics of high temperature (about 300 °C) and high salinity for the Beiya metallogenic fluid, which were origined from magma and probably mixed with some meteoric water in the later period (He, 2014). The ore-forming materials of Beiya deposit were derived from deep-sourced magma according to the isotopic analysis results (He, 2014; Fu et al., 2015; Li et al., 2016).

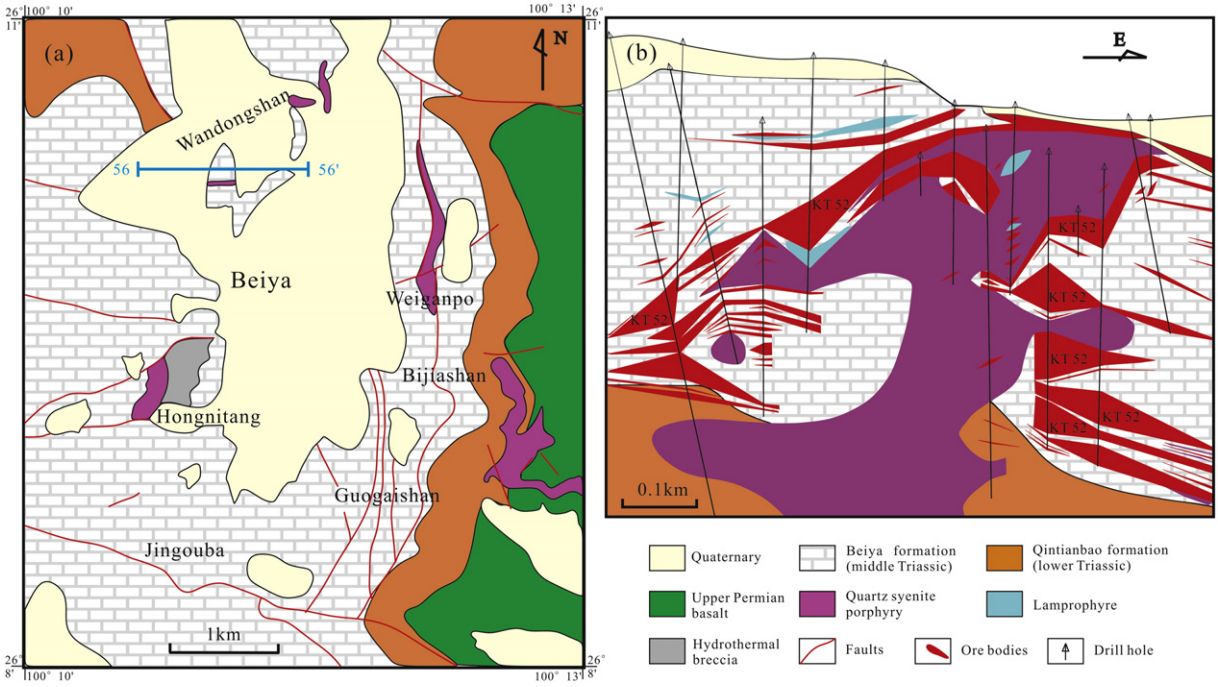

Fig. 2. Geologic map of the Beiya area (a) and the No.56 prospecting line cross section of the Wandongshan ore segment (b). Revised after Xu et al. (2007b) and Lu et al. (2013a).

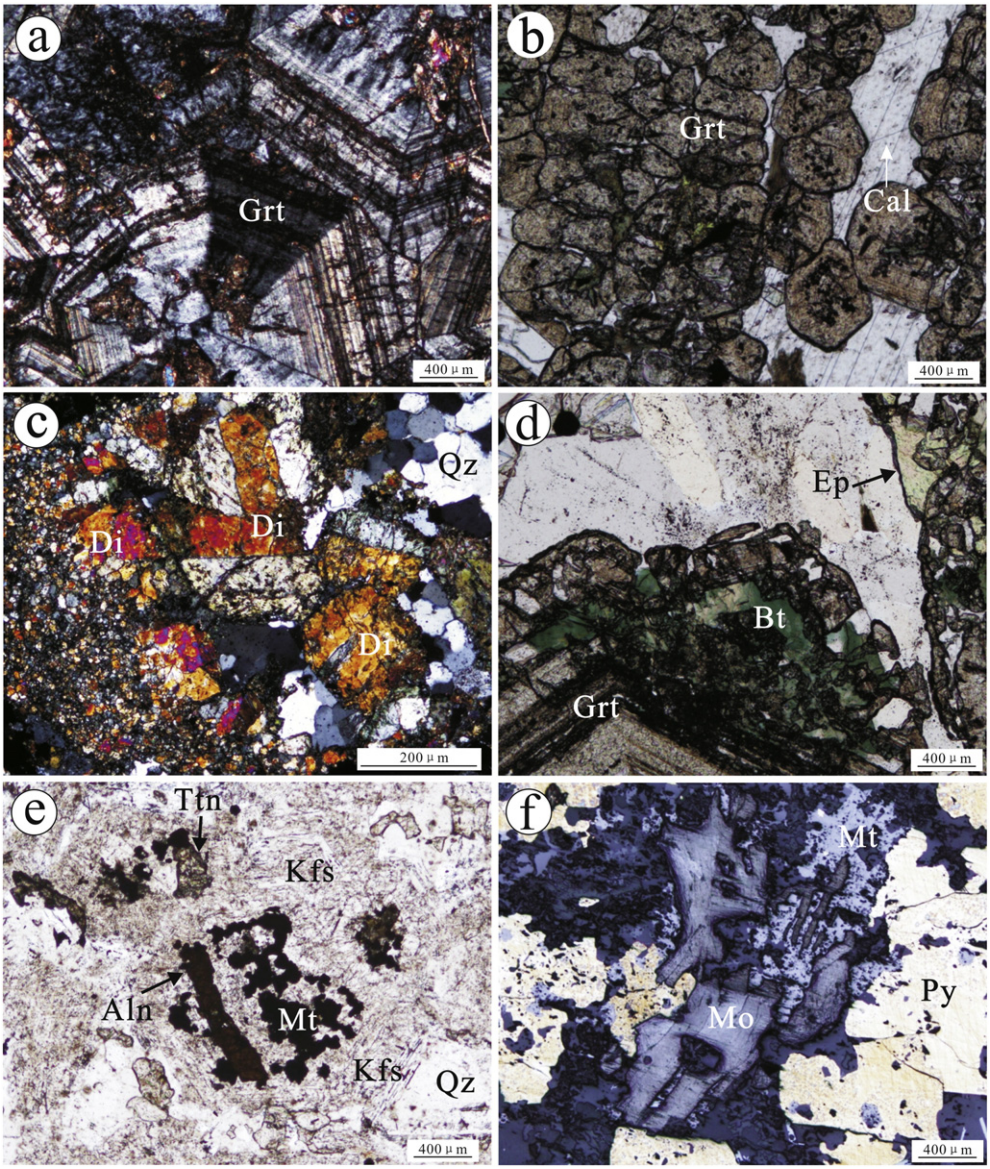

Fig. 3. Photomicrographs of samples in the Beiya deposit. (a–e) Skarn assemblages of garnet, diopside, epidote, biotite, allanite, magnetite and K-feldspar (a and c: cross-polarized light; b, d and e: plane-polarized light). Note that the early garnet was replaced by late magnetite, K-feldspar, titanite and allanite in (e). (f) Molybdenite intergrowth with pyrite and magnetite (reflected light). (Abbreviations: Aln—allanite, Bt—biotite, Di—diopside, Ep—epidote, Grt—garnet, Kfs—K-feldspar, Mo—molybdenite, Mt—magnetite, Pl—plagioclase, Py—pyrite, Qz—quartz, Ttn—titanite, Zrc—zircon.)

3. Samples and analytical methods

Titanite samples for in-situ U–Pb dating and element analysis were collected from the Beiya ore-related porphyry and mineralized skarn. Sample W300 (Fig. 4a) was collected from the ore-related quartz syenite porphyry at Wandongshan, whilst sample W364 (Fig. 4b) was from the cores of 84ZK11 drill hole in the retrograde skarn at Wandongshan, and contains pyroxene, feldspar, quartz, magnetite and minor titanite and allanite. All samples were prepared as standard petrographic thin sections. Petrographic study under the optical microscope was followed by Back-Scattered Electron (BSE) of the titanite, using Zeiss SIGMA field-emission Scanning Electron Microprobe (SEM) at the School of Earth Science and Geological Engineering of Sun Yat-sen University, Guangzhou, China. Prior to LA–ICP–MS analysis, major elements abundance in titanite were determined on thin sections by the JEOL JXA-8800R Electronic Microprobe (EPM) at the Instrumental Analysis & Research Center of Sun Yat-sen University. Operating conditions were 20 kV accelerating voltage and 20 nA beam current with a beam diameter of 2 μm.

Fig. 4. Photographs, photomicrographs and BSE images of porphyry and skarn from the Beiya deposit. (a) titanite-bearing porphyry; (b) titanite-bearing skarn; (c) photomicrographs showing the occurrences of titanite from the Beiya porphyry (cross-polarized light); (d–f) photomicrographs of titanite in skarn (d and e: plane-polarized light; f: cross-polarized light); (g–h) BSE images of titanite in porphyry; (i–j) BSE images of titanite in skarn. (Abbreviations: Di—diopside, Fsp—feldspar, Grt—garnet, Ilm—ilmenite, Mt—magnetite, Pl—plagioclase, Px—pyroxene, Qz—quartz, Rt—rutile, Ttn—titanite, Zrn—zircon.)

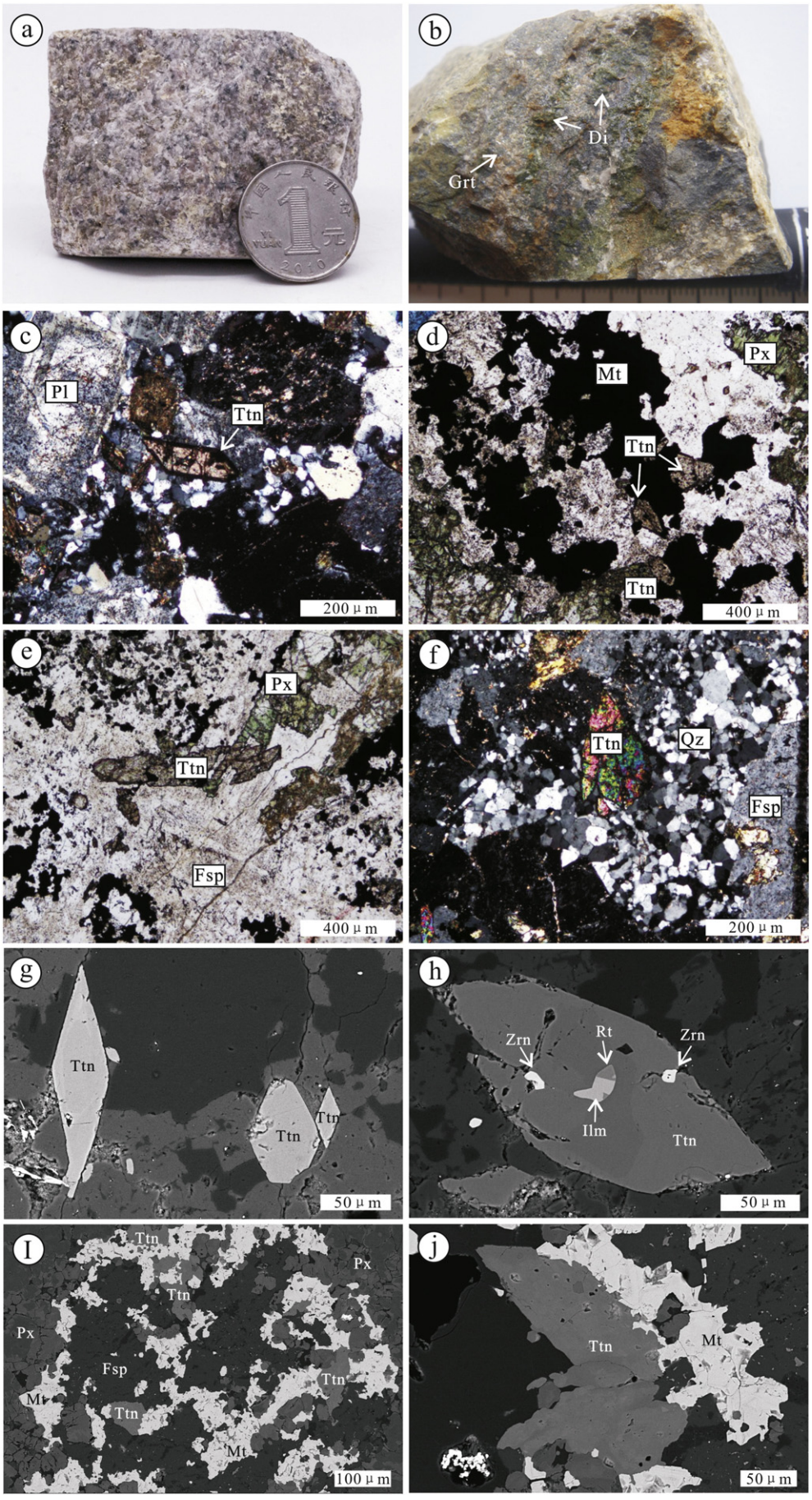
a
b
Di
Grt
c
Pl
Ttn
200 μm
d
Mt
Px
Ttn
Ttn
400 μm
e
Px
Ttn
Fsp
400 μm
f
Ttn
Qz
Fsp
200 μm
g
Ttn
Ttn
Ttn
50 μm
h
Zrn
Rt
Zrn
Ilm
Ttn
50 μm
I
Ttn
Px
Ttn
Px
Fsp
Ttn
Mt
Ttn
Mt
100 μm
j
Ttn
Mt
50 μm

Table 1
Electron microprobe analysis results (wt.%) of the Beiya titanite.

Sample no.	SiO_2	TiO_2	Al_2O_3	FeO	MnO	MgO	CaO	Na_2O	K_2O	F	Total
Magmatic titanite W300											
1	30.04	35.63	1.94	2.27	0.11	–	28.80	0.07	0.01	0.37	99.08
2	30.50	35.28	2.12	2.43	0.09	0.02	28.99	0.03	–	0.77	99.90
3	30.56	35.13	2.39	2.14	0.06	0.02	28.66	0.03	0.01	0.29	99.16
4	32.89	35.45	0.78	2.41	0.04	–	28.69	0.03	0.01	0.11	100.36
5	31.89	36.55	1.31	2.37	0.01	–	27.83	0.02	0.02	0.26	100.13
6	30.80	35.28	1.97	2.85	–	0.02	28.60	0.03	0.01	0.94	100.11
7	32.66	35.78	0.57	2.22	0.08	0.02	28.74	0.08	0.02	0.29	100.34
8	30.74	34.61	2.66	3.16	0.09	0.01	28.74	0.02	–	0.47	100.30
Hydrothermal titanite W364											
1	30.88	32.54	0.83	5.30	0.06	0.03	28.99	–	0.02	1.48	99.50
2	31.40	31.67	3.54	3.08	0.01	0.03	29.27	–	0.03	0.78	99.49
3	30.63	33.60	0.72	4.33	–	0.02	26.37	0.02	0.03	1.20	96.41
4	30.85	33.63	0.64	5.07	0.02	0.01	29.02	0.01	–	0.81	99.73
5	30.83	33.22	1.80	4.81	0.04	–	28.64	0.01	0.05	1.49	100.25
6	31.01	33.00	2.64	4.31	0.06	0.01	28.30	0.01	0.03	0.58	99.70
7	30.92	33.28	1.86	4.91	0.01	0.02	28.29	0.01	0.03	1.15	100.01
8	31.04	31.01	2.65	5.35	0.03	0.03	28.41	–	0.04	1.13	99.19
9	30.82	30.73	2.48	5.93	0.05	0.04	28.60	0.02	–	1.20	99.35
10	30.75	30.93	1.56	5.46	0.02	0.04	28.17	–	–	0.99	97.49
11	29.49	33.44	1.90	4.36	0.05	–	29.40	0.03	0.02	0.51	98.98
12	30.21	30.03	1.33	5.22	0.01	0.05	27.61	0.01	0.01	1.28	95.23
13	29.33	32.58	2.53	3.76	0.01	0.05	29.35	–	–	1.58	98.53
14	29.27	34.54	0.56	4.58	0.03	0.02	29.04	0.02	–	1.09	98.69
15	28.93	35.23	0.57	4.02	0.01	0.03	29.07	0.04	0.02	0.86	98.42
16	35.20	30.68	0.60	5.09	–	0.02	28.50	0.04	–	1.21	100.82
17	30.35	32.42	1.33	5.68	–	0.06	29.11	0.04	–	0.80	99.44
18	30.46	31.13	1.38	6.41	–	0.03	28.98	0.01	–	0.98	98.98
19	31.07	32.94	3.05	3.44	0.05	0.06	29.52	0.03	–	1.69	101.13
20	31.31	30.40	3.48	4.78	–	0.03	30.20	–	0.01	1.18	100.88
21	30.61	32.07	0.47	4.58	–	0.06	29.31	–	0.01	1.54	98.00
22	31.08	30.44	2.75	5.23	0.01	0.04	26.92	–	0.01	1.37	97.27
23	31.44	28.47	3.66	5.87	0.03	0.05	26.72	0.02	–	2.06	97.45
24	31.43	28.24	3.47	6.87	0.01	0.06	27.07	0.02	0.01	1.94	98.30
25	30.61	31.52	2.04	4.86	0.06	0.04	26.17	0.05	0.02	1.27	96.09
26	30.81	31.46	0.60	5.98	0.02	0.03	26.71	0.04	0.02	1.33	96.42
27	30.48	30.94	2.56	3.98	0.05	0.05	26.29	0.04	–	1.62	95.33
28	31.32	31.72	2.62	4.31	0.03	0.03	26.82	–	–	0.78	97.30

In-situ U–Pb dating and trace element analysis of titanite were performed by LA–ICP–MS at the Key Laboratory of Marine Resources and Coastal Engineering, Sun Yat-sen University. Laser sampling was performed using an ArF excimer laser ablation system (GeoLasPro), and ion-signal intensities were acquired using an Agilent 7700× ICP–MS. A 32 μm spot was used with an energy density of 5 J/cm^2 and a repetition rate of 5 Hz. The trace element compositions of titanite were calibrated against the National Institute of Standards and Technology Standard Reference Material 610, using the Ca determined by electron microprobe as the internal standard. Zircon 91,500 was used as the external standard for U–Pb dating. Each analysis consisted of a 20 s background measurement (laser-off) followed by 45 s data acquisition. Data reduction was performed using ICPMSDataCal software (Liu et al., 2010). Meanwhile, ISOPLOT 3.0 software (Ludwig, 2003) was used to construct the Tera–Wasserburg diagram and weighted mean calculations.

The ore-related porphyry in Beiya contains abundant titanite. The titanite grains are about 100–600 μm in length, euhedral and envelope-shaped (Fig. 4c, g, h) with high white interference color (under cross-polarized light). They occur as discrete grains in the interstices of feldspar and quartz, some of which contain inclusions of apatite, zircon, ilmenite and rutile (Fig. 4h). Titanite from the mineralized skarn is mostly subhedral (50–500 μm), and associates with pyroxene, feldspar, magnetite, epidote, quartz and calcite (Fig. 4d–f, i, j). Mineral inclusions of apatite, pyroxene, garnet, quartz and chlorite occur in some titanite. No titanite displays patchy zoning or overgrowth textures in the BSE images, indicating a single mineral growth phase.

4. Results

4.1. Major and trace elements of titanite

Major element geochemical data of titanite are presented in Table 1. Titanite in the ore-related porphyry has relatively uniform SiO_2 (30.04–32.89 wt.%), TiO_2 (34.61–36.55 wt.%), CaO (27.83–28.99 wt.%), Al_2O_3 (0.57–2.66 wt.%) and FeO (2.14–3.16 wt.%). The titanite grains in the mineralized skarn also exhibit uniform SiO_2 (28.93–35.20 wt.%), TiO_2 (28.24–35.23 wt.%), CaO (26.17–30.20 wt.%), Al_2O_3 (0.47–3.66 wt.%) and FeO (3.08–6.87 wt.%). Although CaO contents are very similar for the two titanite types, titanite from the mineralized skarn contains higher F (average: 1.21 wt.%) and FeO (average: 4.91 wt.%), and lower TiO_2 (average: 31.85 wt.%) than titanite in the ore-related porphyry (average: 0.44 wt.%, 2.48 wt.% and 35.47 wt.%, respectively).

Our new titanite trace element geochemical data show that the titanite in skarn is significantly more enriched in HFSEs (e.g., Sn, Y, Nb, Ta, Mo, Th, Zr and Hf) than the titanite in porphyry, with total HFSE concentrations of $10{,}492 \times 10^{-6}$ and 4151×10^{-6} (average values), respectively. The titanite in skarn also has higher U, Lu, Hf and Lu/Hf but lower Th/U (average: 347×10^{-6}, 32.6×10^{-6}, 115.5×10^{-6}, 0.34 and 0.6, respectively) than its porphyry counterpart (average: 43×10^{-6}, 9.4×10^{-6}, 66.8×10^{-6}, 0.18 and 4.6, respectively). In addition, the skarn titanite displays a smaller Light REEs (LREEs) over Heavy REEs (HREEs) enrichment (LREE/HREE ratio values: 1.47–5.59; average: 3.34) and a more prominent negative Eu anomaly (δEu: 0.37–0.59; average: 0.46) than its porphyry counterpart (LREE/HREE ratio values:

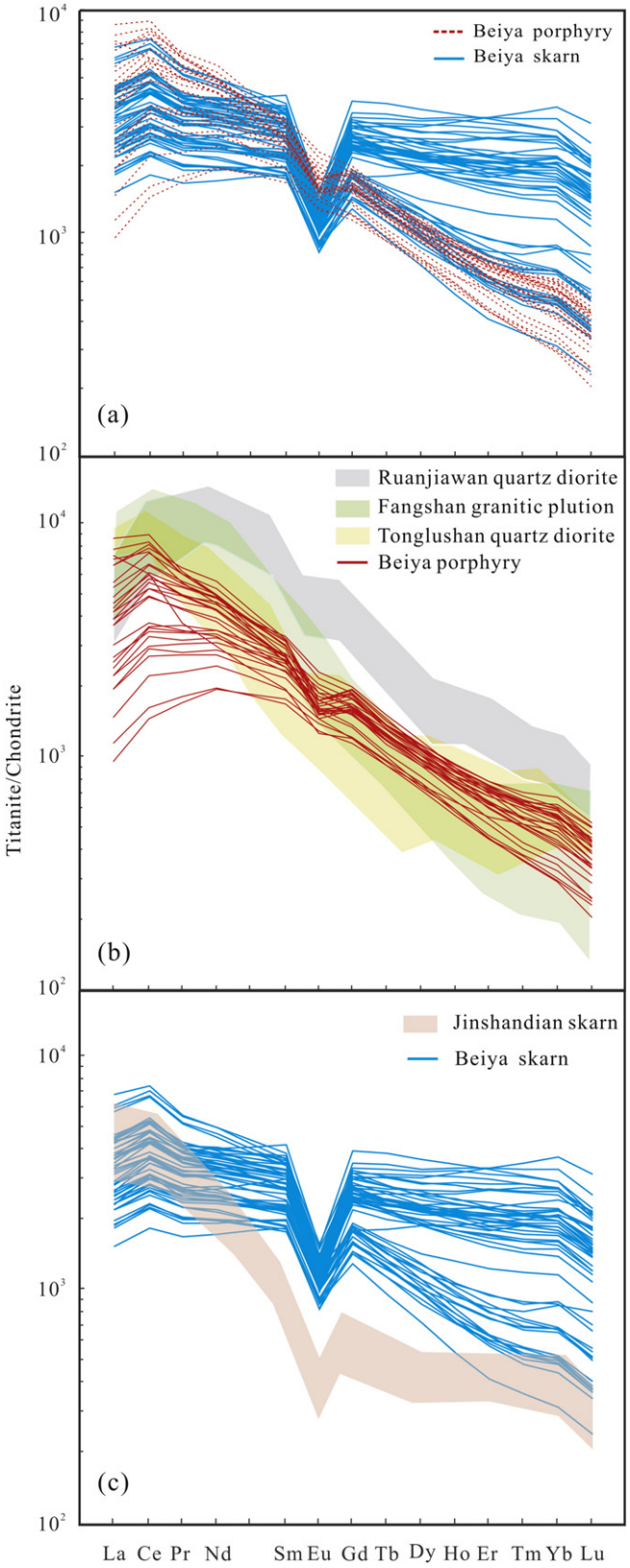

Fig. 5. Chondrite-normalized REE patterns of titanites from ore-related porphyry and mineralized skarn in the Beiya deposit (a) and comparable typical magmatic (b) and hydrothermal ones (c). The gray, green and yellow areas in (b) represent the REE compositions of titanite from the Ruanjiawan diorite (Deng et al., 2015a), Fangshan granitic pluton (Sun et al., 2010) and Tonglushan diorite (Li et al., 2010), respectively; the pink area in (c) represents the REE compositions of titanite from the Jinshandian skarn (Zhu et al., 2014). (Chondrite value is from Sun and McDonough, 1989.)

3.87–11.82; average: 7.64 and δEu: 0.68–0.94; average: 0.80) (Fig. 5 and Table 2).

4.2. Titanite U–Pb age

Most zircon and some titanite contain negligible common Pb and thus the Stacey and Kramers (1975)'s model for correction of Pb isotopic data is applicable. However, for the titanite with higher common Pb (percentage of common $^{206}Pb > 10\%$), use of a model Pb isotopic composition may be inappropriate (Aleinikoff et al., 2002). Moreover, if the titanite is young or has low U and Pb concentrations, the choice of initial Pb isotopic composition will influence the calculated ages significantly (Frost et al., 2000). In this study, our samples are young and have high common Pb, indicating that the ^{207}Pb-correction method, which is more precise for common Pb correction should be adopted (Stern, 1997; Aleinikoff et al., 2002). The uncorrected data are plotted in the Tera–Wasserburg diagram (Fig. 6), and a regression through these analyses yields a lower intercept that represents the approximate titanite age. The y-intercept represents the initial $^{207}Pb/^{206}Pb$ (Aleinikoff et al., 2002), which can be used in an algorithm to allow a form of ^{207}Pb-correction (Stern, 1997; Frost et al., 2000). Subsequently, the individual ^{207}Pb-corrected $^{206}Pb/^{238}U$ ages can be calculated for the weighted average age, which represents the real age of titanite. This approach has been shown effective in correcting common-Pb of titanite (Storey et al., 2006).

U–Pb isotope results of titanite in the Beiya mineralized skarn are listed in Table 3. On the Tera–Wasserburg diagram, the common Pb-uncorrected data define a linear array, giving a lower-intercept age of 33.7 ± 1.2 Ma (MSWD = 1.2), and the y-intercept of initial $^{207}Pb/^{206}Pb$ at 0.8408 (Fig. 6a). With this common Pb composition, common Pb correction was conducted using the ^{207}Pb-based method. All analyses yielded a weighted average $^{206}Pb/^{238}U$ age of 33.1 ± 1.0 Ma (MSWD = 2.0) (Fig. 6a), consistent with the lower-intercept age within the error range. The titanite U–Pb isotope data for the ore-related porphyry are listed in Table 4. They exhibit lower U and Pb with higher common Pb (all data points plot far away from the lower intercept), resulting in greater experimental errors, and thus the lower intercept age (36.0 ± 5.9 Ma) is used as the titanite age.

5. Discussion

5.1. Origin of titanite

Different origins of titanite can be discriminated by their texture, paragenetic mineral assemblages and geochemistry (Cao et al., 2015). The titanite grains in the Beiya mineralized skarn are mostly subhedral, and commonly coexist with typical retrograde skarn minerals including magnetite, feldspar, pyroxene and quartz, suggesting a hydrothermal origin. In contrast, titanite grains from the Beiya ore-related porphyry are all euhedral envelope-shaped, and occur in the interstices of feldspar and quartz phenocrysts, implying a magmatic origin. This conclusion is further supported by the titanite geochemistry. Both Fig. 7a and b show good negative correlation between TiO_2 and F, TiO_2 and $FeO + Al_2O_3$, respectively. Consequently, the dominant substitution mechanism in our data is likely to be: $(Al, Fe)^{3+} + (F, OH)^{-} = Ti^{4+} + O^{2-}$, consistent with previous studies (Cempírek et al., 2008; Horie et al., 2008; Olin and Wolff, 2012; Che et al., 2013; Cao et al., 2015). As demonstrated in Fig. 7, titanite from the Beiya ore-related porphyry shows low F, Al, Fe and high Ti, and all the data points fall on the upper left hand part of the diagram, resembling typical magmatic titanite. In contrast, titanite from the mineralized skarn falls on the lower right hand part of the diagram with high F, Al, Fe and low Ti contents, exhibiting the characteristics of hydrothermal titanite (Broska et al., 2007; Morad et al., 2009; Li et al., 2010; Che et al., 2013).

Th/U ratio in titanite is useful for investigating the origin of titanite. In general, hydrothermal titanite has lower Th/U (mostly <1) than

Table 2
Trace element analysis result ($\times 10^{-6}$) of the Beiya titanite by LA–ICP–MS.

Sample no.	Zr	Nb	Mo	Sn	Hf	Ta	Th	U	Y	La	Ce	Pr	Nd	Sm	Eu	Gd	Tb	Dy	Ho	Er	Tm	Yb	Lu	HFSE	ΣREE	LREE/HREE	δEu	δCe	Th/U	Y/Ho	Nb/Ta	Lu/Hf
Hydrothermal titanite																																
w364-01	3439	1976	59.1	1098	197.9	58.5	129	268	4110	1027	3132	379	1750	530	85.9	624	111.9	720	162	462	72.4	458	53.8	11,067	9567	2.59	0.46	1.23	0.5	25.4	33.8	0.27
w364-02	9089	2080	61.3	3616	385.0	88.5	252	327	3965	1059	3301	391	1890	543	73.6	625	102.4	644	138	371	53.0	333	37.6	19,536	9560	3.15	0.39	1.26	0.8	28.8	23.5	0.10
w364-03	2530	1497	67.6	1948	78.7	46.7	178	183	3623	943	2917	365	1693	491	69.3	560	97.5	605	130	368	53.5	346	39.6	9969	8676	2.95	0.40	1.22	1.0	27.8	32.1	0.50
w364-04	1533	1484	70.7	1732	61.4	37.3	200	245	3178	902	2702	347	1612	471	66.1	509	85.6	541	115	322	47.3	313	36.9	8296	8070	3.10	0.41	1.18	0.8	27.8	39.8	0.60
w364-05	2253	1805	78.3	1873	86.8	63.7	172	188	4687	940	2874	364	1692	520	77.6	647	115.3	777	172	489	71.9	460	50.9	11,018	9250	2.32	0.41	1.20	0.9	27.3	28.3	0.59
w364-06	1850	1609	70.4	672	82.5	45.1	61	345	1355	521	1618	222	1087	329	59.7	325	46.4	248	44	104	14.4	87	10.1	5744	4716	4.36	0.55	1.17	0.2	30.7	35.6	0.12
w364-07	1674	1768	85.8	716	63.1	45.6	39	347	1685	553	1702	239	1145	353	63.2	376	55.1	306	55	132	17.6	115	12.5	6075	5123	3.79	0.53	1.15	0.1	30.8	38.8	0.20
w364-08	2791	1597	69.6	1860	99.3	51.9	148	241	3508	736	2225	295	1422	416	66.4	508	91.0	586	131	367	54.9	369	45.2	10,124	7313	2.40	0.44	1.17	0.6	26.8	30.8	0.45
w364-09	1995	1291	86.8	520	59.5	49.9	51	223	1188	461	1418	190	919	267	51.6	295	42.2	229	41	100	14.2	85	9.5	5241	4121	4.06	0.56	1.17	0.2	29.3	25.9	0.16
w364-10	2060	1888	83.2	626	55.0	34.5	34	329	1721	572	1710	235	1104	339	60.9	364	52.8	306	53	131	18.5	114	12.9	6501	5075	3.82	0.53	1.14	0.1	32.3	54.8	0.23
w364-11	2818	1134	64.7	559	68.4	28.1	24	173	1324	447	1367	189	923	301	52.9	318	46.7	243	40	94	12.1	74	8.6	6021	4117	3.92	0.52	1.15	0.1	32.8	40.3	0.13
w364-12	7653	1714	89.8	897	202.8	73.4	50	242	1741	616	1866	250	1161	338	59.1	385	58.7	325	58	142	18.8	116	13.6	12,421	5406	3.84	0.50	1.17	0.2	30.0	23.3	0.07
w364-13	3527	1622	126.5	992	123.6	55.9	97	380	1684	765	2249	295	1354	364	71.0	365	56.1	320	60	154	22.5	145	16.7	8228	6238	4.47	0.59	1.16	0.3	28.0	29.0	0.14
w364-14	3535	1475	91.3	689	107.9	45.0	36	308	1432	553	1668	228	1126	362	66.0	374	53.2	277	46	105	13.3	84	9.3	7411	4965	4.16	0.54	1.15	0.1	31.0	32.8	0.09
w364-15	3182	1099	71.7	2834	103.4	37.0	241	193	2936	1025	2919	362	1621	409	56.2	451	74.4	480	105	292	47.1	303	37.2	10,504	8180	3.57	0.40	1.17	1.2	28.0	29.7	0.36
w364-16	12,117	2019	55.3	4776	374.7	85.2	353	442	3281	1410	4154	487	2161	532	66.6	556	90.7	559	116	320	47.2	303	35.0	23,061	10,837	4.35	0.37	1.22	0.8	28.3	23.7	0.09
w364-17	3214	1320	76.5	2096	139.8	46.7	180	283	4152	755	2257	305	1473	438	68.0	524	95.7	648	145	436	69.0	452	53.3	11,225	7720	2.18	0.43	1.15	0.6	28.5	28.3	0.38
w364-18	2582	1465	85.2	1447	88.4	33.2	143	333	2642	881	2622	349	1650	478	79.3	511	79.9	475	95	250	36.4	236	27.3	8486	7771	3.54	0.49	1.16	0.4	27.9	44.1	0.31
w364-19	1950	1482	95.0	1422	82.7	40.6	194	283	2916	855	2560	340	1559	454	72.6	496	80.5	492	100	282	41.5	276	31.8	8182	7640	3.24	0.46	1.16	0.7	29.2	36.5	0.38
w364-20	2551	1781	101.7	1818	92.5	43.4	207	473	3310	853	2579	342	1616	475	75.6	526	87.1	560	122	348	52.2	351	39.5	9904	8027	2.85	0.46	1.17	0.4	27.2	41.1	0.43
w364-21	2444	1406	95.8	1695	84.5	32.2	199	417	2774	1002	2947	380	1722	465	77.4	508	81.0	485	101	273	40.4	263	30.4	8731	8374	3.70	0.48	1.17	0.5	27.5	43.7	0.36
w364-22	2611	1683	91.9	1458	92.5	45.1	188	454	4070	801	2370	319	1541	479	77.2	568	100.9	671	148	445	66.5	445	52.6	10,239	8085	2.24	0.45	1.15	0.4	27.4	37.4	0.57
w364-23	3952	1819	104.2	2207	119.5	49.9	294	507	2896	1084	3217	402	1830	478	69.4	501	81.9	483	100	280	40.8	271	30.4	11,440	8869	3.96	0.43	1.19	0.6	28.9	36.5	0.25
w364-24	2977	1784	74.4	901	105.6	56.8	96	356	1300	552	1689	229	1101	331	57.7	325	45.6	245	42	103	13.4	85	9.3	7294	4828	4.56	0.53	1.16	0.3	31.0	31.4	0.09
w364-25	3010	1535	84.7	1154	107.9	67.6	97	387	2131	667	1980	265	1230	342	61.7	391	60.4	359	74	202	30.2	195	22.2	8188	5878	3.41	0.51	1.15	0.3	28.7	22.7	0.21
w364-26	6264	1709	64.9	1051	138.2	39.0	378	286	3560	618	2134	288	1414	403	63.1	502	85.2	543	120	342	53.9	365	46.7	13,204	6977	2.39	0.43	1.24	1.3	29.7	43.9	0.34
w364-27	9606	2176	67.6	1190	209.9	65.4	326	294	3632	685	2276	303	1501	434	67.5	529	89.0	566	120	341	52.1	344	41.4	17,273	7348	2.53	0.43	1.22	1.1	30.2	33.3	0.20
w364-28	1713	1152	76.6	588	43.9	19.6	526	304	3879	539	1875	259	1281	391	62.8	480	84.0	558	125	371	59.4	411	54.6	7998	6551	2.06	0.44	1.23	1.7	31.1	58.9	1.25
w364-29	1432	1319	75.5	544	54.8	40.9	77	206	1473	444	1412	192	930	277	47.7	296	45.0	250	48	122	17.5	115	14.1	5015	4210	3.64	0.51	1.18	0.4	30.5	32.2	0.26
w364-30	2517	2353	98.2	773	72.0	57.2	58	394	1443	604	1841	246	1155	349	61.8	360	49.6	260	44	103	13.3	82	9.1	7371	5177	4.62	0.53	1.17	0.1	32.9	41.1	0.13
w364-31	5239	2001	89.5	760	113.8	46.9	287	536	1651	592	1899	247	1177	325	57.6	342	49.9	277	53	137	20.4	144	20.3	10,188	5342	4.12	0.52	1.22	0.5	31.4	42.7	0.18
w364-32	3845	2252	83.0	3407	96.1	42.1	383	1491	4511	1084	3245	392	1847	557	80.8	657	113.7	728	157	437	65.9	428	49.5	14,619	9841	2.73	0.41	1.22	0.3	28.8	53.5	0.51
w364-33	2708	1357	70.5	1611	96.0	40.3	193	257	3562	860	2695	334	1529	433	59.7	493	85.2	554	118	338	52.6	345	40.2	9638	7936	2.92	0.39	1.23	0.8	30.3	33.7	0.42
w364-34	3246	1624	82.9	973	78.9	24.2	447	392	3566	665	2181	289	1407	407	64.3	485	81.6	531	116	342	53.2	365	45.7	10,043	7032	2.48	0.44	1.22	1.1	30.7	67.2	0.58
w364-35	1969	1754	81.4	596	64.7	40.4	78	336	1246	515	1603	213	1009	286	49.6	290	41.5	220	40	98	13.1	87	9.7	5830	4474	4.60	0.52	1.19	0.2	31.1	43.4	0.15
w364-36	1712	2502	85.5	664	51.4	40.9	63	312	1355	587	1864	234	1118	320	56.7	330	46.5	245	42	97	12.7	81	9.2	6474	5044	4.84	0.53	1.23	0.2	32.3	61.2	0.18
w364-37	8652	2216	55.8	4052	221.8	80.3	313	221	3821	1446	4351	518	2304	584	75.6	646	103.2	632	132	358	52.8	332	39.0	19,412	11,573	4.04	0.37	1.23	1.4	29.0	27.6	0.18
w364-38	11,306	4158	63.1	5545	218.8	129.5	397	1286	3550	1622	4582	530	2291	544	70.3	584	95.5	585	123	346	50.9	333	38.0	25,368	11,794	4.47	0.38	1.21	0.3	28.8	32.1	0.17
w364-39	9254	3387	62.1	4882	181.6	78.2	315	560	3392	1350	4044	482	2085	515	67.9	561	90.0	558	116	323	48.4	311	36.0	21,552	10,588	4.18	0.38	1.23	0.6	29.2	43.3	0.20

w364-40	4608	1734	91.2	2813	117.1	36.0	385	431	5339	1039	3223	395	1859	566	77.7	714	127.7	830	187	546	83.5	554	64.1	15,124	10,268	2.30	0.37	1.23	0.9	28.5	48.1	0.55
w364-41	2395	2544	116.6	1752	82.5	83.7	173	212	5543	813	2728	370	1865	631	88.5	800	141.5	912	193	538	78.2	492	52.8	12,691	9703	2.02	0.38	1.22	0.8	28.8	30.4	0.64
w364-42	1336	1487	100.8	976	58.9	59.6	124	217	5426	565	1809	248	1247	449	80.0	609	112.8	763	179	547	87.9	623	78.5	9568	7397	1.47	0.47	1.18	0.6	30.4	25.0	1.33
w364-43	2437	1644	102.6	1279	79.9	28.5	211	277	2993	783	2550	326	1495	430	68.0	483	78.4	475	97	261	37.8	252	29.3	8774	7366	3.30	0.45	1.24	0.8	30.8	57.7	0.37
w364-44	2257	1688	94.9	1549	87.7	31.5	210	373	3395	845	2691	339	1583	462	70.3	548	86.5	545	115	309	47.6	303	36.4	9314	7982	3.01	0.43	1.23	0.6	29.6	53.6	0.41
w364-45	4741	1922	55.2	2842	160.8	54.7	151	217	4118	995	3111	383	1779	520	72.9	610	103.0	660	137	388	57.0	375	43.1	14,045	9234	2.89	0.39	1.23	0.7	30.0	35.1	0.27
w364-46	2856	1391	66.7	1968	100.9	32.8	143	175	3636	856	2620	326	1560	456	65.0	532	90.7	571	119	333	48.8	324	36.6	10,196	7937	2.86	0.40	1.22	0.8	30.6	42.4	0.36
w364-47	3451	1868	118.9	1357	102.7	47.7	198	241	3466	880	2891	368	1732	497	74.7	542	89.1	543	110	297	43.9	289	34.5	10,609	8391	3.31	0.44	1.25	0.8	31.4	39.2	0.34
w364-48	2016	999	73.7	503	59.8	28.6	67	236	1472	433	1349	181	890	303	52.0	322	48.9	268	49	125	17.0	111	12.8	5219	4161	3.36	0.51	1.18	0.3	29.8	34.9	0.21
w364-49	1561	2934	88.5	449	49.7	154.0	77	229	967	515	1559	213	997	282	51.1	263	35.3	183	30	68	9.0	53	6.1	6280	4264	5.59	0.56	1.15	0.3	32.1	19.1	0.12
w364-50	2648	1290	60.0	913	98.8	44.8	76	291	1625	625	1891	255	1207	344	57.1	365	52.6	301	59	156	22.1	150	17.9	6755	5503	3.90	0.49	1.16	0.3	27.6	28.8	0.18
w364-51	3091	2204	59.3	777	193.7	64.1	123	233	4482	1028	3139	387	1791	558	89.8	679	122.1	808	181	518	76.9	491	56.3	10,993	9924	2.38	0.45	1.22	0.5	24.8	34.4	0.29
w364-52	980	1021	51.4	1047	54.3	45.7	99	192	2967	360	1118	159	800	278	47.8	363	67.1	470	105	320	50.8	353	46.0	6266	4538	1.56	0.46	1.14	0.5	28.3	22.3	0.85
w364-53	5207	1428	79.4	1079	170.9	41.1	251	256	3113	658	2117	295	1427	413	67.9	468	79.9	503	108	303	45.6	294	35.7	11,370	6816	2.71	0.47	1.18	1.0	28.8	34.7	0.21
Magmatic titanite																															
W300-01	455	1198	34.8	137	32.0	99.9	242	53	1400	985	3524	502	2219	471	100.9	384	50.7	269	49	121	16.4	102	11.1	3598	8805	7.78	0.70	1.22	4.5	28.5	12.0	0.35
W300-02	1380	903	23.2	107	74.2	53.1	147	37	1307	916	2952	400	1753	368	90.9	323	45.6	256	46	120	16.0	94	10.3	3995	7391	7.11	0.79	1.19	4.0	28.4	17.0	0.14
W300-03	2880	1252	21.3	161	162.0	100.7	222	49	1328	1256	4049	531	2314	450	108.2	368	51.1	276	50	125	15.8	95	10.6	6127	9699	8.80	0.79	1.22	4.5	26.8	12.4	0.07
W300-04	1402	702	7.0	73	60.7	64.1	137	20	1020	623	2081	320	1553	365	100.3	314	43.7	236	41	100	12.7	70	8.7	3466	5871	6.10	0.88	1.13	6.7	24.7	11.0	0.14
W300-05	864	404	3.5	54	39.4	49.6	82	16	704	270	992	171	916	256	74.2	234	34.4	182	31	73	9.1	50	5.8	2200	3298	4.32	0.91	1.10	5.1	22.5	8.1	0.15
W300-06	1221	368	2.7	54	46.4	22.4	89	16	743	224	886	161	902	267	80.5	248	35.6	195	33	73	9.5	51	6.1	2546	3173	3.87	0.94	1.10	5.5	22.3	16.4	0.13
W300-07	710	883	36.5	104	40.0	64.3	173	48	1171	859	3162	434	1964	402	90.3	318	45.1	237	43	107	13.7	86	9.6	3181	7772	8.03	0.74	1.26	3.6	27.0	13.7	0.24
W300-08	540	994	34.8	124	35.7	64.1	203	41	1323	1557	4918	579	2299	417	90.3	341	46.0	256	48	119	15.7	99	10.9	3318	10,795	10.55	0.71	1.27	5.0	27.6	15.5	0.31
W300-09	523	954	31.7	125	34.3	68.0	207	47	1335	1319	4580	569	2413	483	100.4	398	53.6	275	50	118	16.4	94	11.3	3278	10,480	9.31	0.68	1.30	4.4	26.4	14.0	0.33
W300-10	445	844	30.7	114	31.7	61.0	197	47	1227	1137	4002	515	2221	457	97.9	373	49.2	261	47	117	15.7	91	9.7	2951	9394	8.76	0.70	1.28	4.2	26.3	13.8	0.31
W300-11	2280	650	11.7	98	96.4	53.8	139	27	1055	525	1823	287	1428	382	104.7	341	51.2	280	49	114	13.8	78	8.7	4384	5486	4.87	0.87	1.14	5.2	21.6	12.1	0.09
W300-12	1411	1028	36.7	130	74.2	67.9	141	133	947	1710	3683	352	1373	294	72.9	244	34.3	191	36	91	13.0	81	9.2	3837	8186	10.70	0.81	1.10	1.1	26.5	15.1	0.12
W300-13	1074	991	24.4	106	55.8	80.9	237	40	1194	985	3195	458	2134	495	131.9	408	55.7	294	50	118	14.7	84	9.0	3763	8432	7.16	0.87	1.16	5.9	23.7	12.3	0.16
W300-14	625	540	17.3	84	38.5	36.9	125	27	841	710	2268	328	1517	348	93.8	281	38.6	208	36	84	10.2	59	6.2	2308	5989	7.28	0.89	1.15	4.6	23.2	14.6	0.16
W300-15	554	362	15.5	41	26.2	27.1	134	25	1054	599	2189	345	1627	394	109.0	332	46.7	246	44	103	12.9	73	8.4	2213	6129	6.08	0.90	1.16	5.4	24.2	13.4	0.32
W300-16	931	703	5.4	70	39.8	71.2	104	19	733	459	1627	259	1265	328	89.4	272	37.1	191	33	74	9.1	49	5.1	2657	4697	6.01	0.89	1.14	5.6	22.4	9.9	0.13
W300-17	690	1096	31.6	120	35.8	82.0	176	51	1188	856	2937	410	1824	405	91.5	334	45.6	242	42	102	13.9	78	8.7	3420	7390	7.54	0.74	1.21	3.4	28.1	13.4	0.24
W300-18	1451	3378	27.2	219	81.0	182.2	250	95	1337	2029	5424	589	2302	457	100.2	391	52.5	284	51	128	17.8	113	13.1	6925	11,952	10.37	0.71	1.20	2.6	26.1	18.5	0.16
W300-19	11,083	1140	37.4	128	255.7	81.1	230	82	1274	1652	4606	528	2119	402	87.2	337	46.1	248	46	116	16.2	105	12.7	14,229	10,321	10.13	0.70	1.20	2.8	27.5	14.1	0.05
W300-20	1266	713	5.0	80	60.2	76.6	128	18	855	459	1758	264	1336	355	100.5	307	43.4	232	39	90	10.9	62	7.2	3184	5063	5.40	0.91	1.22	7.0	21.8	9.3	0.12
W300-21	1565	984	6.6	98	70.8	108.0	163	25	930	525	1999	299	1493	393	112.6	336	48.8	256	44	98	12.5	69	7.7	3925	5694	5.53	0.92	1.22	6.6	21.3	9.1	0.11
W300-22	1744	939	8.4	97	86.1	83.2	175	28	999	561	2166	323	1616	419	117.3	359	50.6	267	46	105	13.0	74	8.5	4131	6125	5.63	0.90	1.23	6.2	21.7	11.3	0.10
W300-23	2156	687	12.9	75	57.8	46.8	117	23	1270	1554	4768	604	2615	488	124.6	384	50.1	271	51	124	15.9	93	11.0	4424	11,152	10.16	0.85	1.21	5.2	25.1	14.7	0.19
W300-24	802	946	29.0	118	49.9	64.1	187	51	1201	1813	5101	578	2261	389	87.2	316	41.8	232	44	112	15.2	93	10.9	3398	11,095	11.82	0.74	1.21	3.7	27.4	14.8	0.22
W300-25	422	965	31.8	119	29.5	68.5	199	48	1204	1069	3627	465	1981	409	86.5	330	45.6	247	45	112	15.1	88	10.4	3038	8532	8.55	0.70	1.26	4.2	26.5	14.1	0.35
W300-26	1292	1030	27.8	132	52.5	75.6	206	50	1330	913	3412	468	2065	443	94.5	361	49.1	271	50	125	16.6	100	11.7	4146	8380	7.51	0.70	1.27	4.1	26.4	13.6	0.22
W300-27	6142	1197	31.6	140	167.9	98.9	235	64	1356	1018	3762	506	2245	477	100.3	379	51.4	284	52	128	17.2	103	12.4	9368	9135	7.89	0.70	1.28	3.7	25.9	12.1	0.07
W300-28	1408	975	35.5	115	51.0	68.9	196	50	1142	1072	3657	462	1960	394	83.9	323	44.3	237	43	106	14.0	85	10.0	3991	8490	8.85	0.70	1.27	3.9	26.6	14.2	0.20
W300-29	1056	363	5.0	50	51.2	36.3	71	14	736	349	1352	218	1138	293	83.4	245	35.1	186	33	75	9.6	55	6.3	2369	4079	5.32	0.92	1.17	5.0	22.1	10.0	0.12

Note: $\delta Eu = (Eu/Eu^*)_N = Eu_N/2(Sm_N + Gd_N)$; $\delta Ce = (Ce/Ce^*)_N = Ce_N/2(La_N + Pr_N)$; LREE = La + Ce + Pr + Nd + Sm + Eu; HREE = Gd + Tb + Dy + Ho + Er + Tm + Yb + Lu.

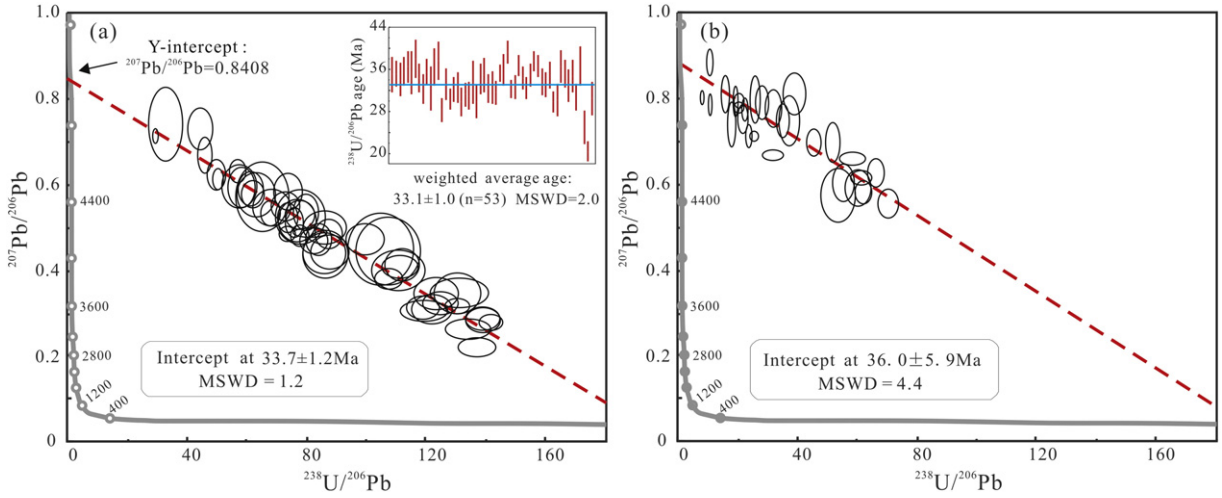

Fig. 6. Tera–Wasserburg diagram for the titanite in skarn (a) and porphyry (b) from the Beiya deposit.

magmatic titanite (Aleinikoff et al., 2002; Gao et al., 2012; Che et al., 2013; Deng et al., 2015a). In our study, the mineralized-skarn titanite yielded low Th/U (0.1–0.7; average: 0.6), indicating a typical hydrothermal origin and is comparable with the hydrothermal titanite from the Ruanjiawan W–Cu–Mo skarn and Tonglushan Cu–Au–Fe skarn deposits (Th/U ratio values: 0.01–0.29 and 0.03–3.22, respectively) in the Daye district, Eastern China (Li et al., 2010; Deng et al., 2015a). In contrast, Th/U of the Beiya ore-related porphyry titanite is much higher than 1 (1.1–7.0; average: 4.6), suggesting a magmatic origin. The Beiya hydrothermal titanite contains higher Lu/Hf (average: 0.34) than magmatic titanite (average: 0.18), similar with the hydrothermal titanite in scapolite skarn from the Jinshandian Fe skarn deposit (Lu/Hf ratio values: 0.16–0.78; average: 0.42) in Hubei province, Central China (Zhu et al., 2014). These, together with the higher HFSE contents and Nb/Ta of hydrothermal titanite than magmatic titanite, point to a different origin for these two titanite types.

REE characteristics of titanite are good indicator for its origin. Titanite in the Beiya porphyry displays right-dipping REE patterns, high ΣREE contents and slightly negative Eu anomaly (Fig. 5a), resembling typical magmatic titanite and similar with the magmatic titanite in quartz diorite from the Tonglushan Cu–Au–Fe skarn and Ruanjiawan W–Cu–Mo skarn deposits, as well as with that in the Fangshan granitic pluton in North China Craton (Fig. 5b) (Li et al., 2010; Sun et al., 2010; Deng et al., 2015a). The titanite in the Beiya mineralized skarn, in contrast, shows lower LREE/HREE enrichment and a more distinct Eu anomaly (Fig. 5a). These features are comparable with hydrothermal titanite from the Jinshandian skarn deposit (Fig. 5c) (Zhu et al., 2014). The aqueous solutions are generally depleted in fluid-mobile incompatible trace elements such as LREE relative to hydrous melts (Hermann et al., 2006), which might lead to the growth of hydrothermal titanite with lower LREE/HREE ratios. The negative Eu anomaly of Beiya magmatic titanite may have been caused by the fractionation of plagioclase that preferentially incorporates Eu (Deng et al., 2015a). For the hydrothermal titanite, this is especially important in an oxidizing condition, where Eu^{2+} is oxidized into Eu^{3+} and becomes less incorporated into titanite (Horie et al., 2008), leading to a distinct negative Eu anomaly. Therefore, the prominent negative Eu anomaly of the Beiya hydrothermal titanite indicates that the ore forming fluids are relatively oxidized. As a whole, the similar right-dipping REE pattern and ΣREE of the hydrothermal- and magmatic titanite suggest that the hydrothermal source of mineralized skarn in the Beiya deposit might be magmatic fluids (Li et al., 2010; Cao et al., 2015).

In Fig. 8, it's noted that the trace elements compositions of magmatic and hydrothermal titanites are quite distinct, thus can be also used to identify their origin. Generally speaking, LREE/HREE ratios in the magmatic titanite are higher than those in the hydrothermal titanite, therefore all data points fall on the upper right hand part of the Fig. 8a. While the hydrothermal titanite usually have higher Nb/Ta ratios and HFSEs contents in a larger scope, with all the data points falling on the upper left hand part of the Fig. 8b and d. The Lu/Hf ratio cannot tell the origin of titanite without other evidences, for it varies by different deposits (Fig. 8c).

5.2. Geochronology of the Beiya deposit

Titanite U–Pb dating has been mainly applied to magmatic- and metamorphic rocks but less commonly to hydrothermal mineralization. Dating hydrothermal minerals places direct age constraints on hydrothermal activities and the associated metallogeny, a crucial aspect in ore deposit study. Hence, U–Pb dating of hydrothermal titanite has received increasingly more attention (Chiaradia et al., 2009; Smith et al., 2009; Li et al., 2010; Fallourd et al., 2014; Cao et al., 2015; Chelle-Michou et al., 2015; Deng et al., 2015a). In this study, magmatic titanite yields an intercept age of 36.0 ± 5.9 Ma, consistent with the Beiya ore-related porphyry (zircon U–Pb: 36.07 ± 0.43 Ma) formation age (Fu et al., 2015). The hydrothermal titanite from Beiya skarn was formed during the retrograde skarn alteration, which was followed by the quartz–sulfide alteration and the gold mineralization. Therefore, the gold mineralization age is not older than the formation time of titanite. That is to say, the ore forming age of the Beiya deposit is around or slightly younger than 33.1 ± 1.0 Ma (32.1–34.1 Ma). Previous research has indicated that the mineralization in the Beiya deposit took place at 34.7 ± 1.6 Ma (33.1–36.3 Ma) according to the molybdenite Re–Os dating analysis (Fu et al., 2015), which seems to be older than the formation time of titanite. Since the results were obtained using different experimental subjects and analysis methods, we should take the errors into consideration when calculating the mineralization age (not older than 34.1 Ma and also between 33.1 Ma and 36.3 Ma). As a result, high-precision ages from retrograde skarn (U–Pb, hydrothermal titanite) and later-stage mineralization (Re–Os, molybdenite) in the Beiya deposit all together constrain the Beiya mineralization to between 33.1 and 34.1 Ma, just slightly younger than the porphyry emplacement (36.07 ± 0.43 Ma) (Fu et al., 2015). The close temporal relationship between the mineralization and the alkaline porphyry suggests that the Beiya gold–polymetallic metallogeny was likely to be caused by post-magmatic hydrothermal activities in the Himalayan orogenic event.

Table 3
LA–ICP–MS U–Pb isotope data for hydrothermal titanite from the Beiya deposit.

Sample no. W364	Pb	Th	U	Measured isotopic ratios						^{207}Pb-corrected ages (Ma)	
	$\times 10^{-6}$			^{207}Pb/^{206}Pb	1σ	^{207}Pb/^{235}U	1σ	^{206}Pb/^{238}U	1σ	^{206}Pb/^{238}U	1σ
01	3.8	129	268	0.2623	0.0207	0.2700	0.0193	0.0075	0.0003	35.00	3.32
02	12.4	252	327	0.5127	0.0268	0.9327	0.0481	0.0132	0.0004	35.08	2.40
03	9.3	178	183	0.5759	0.0284	1.2595	0.1142	0.0159	0.0011	34.04	3.13
04	7.7	200	245	0.4725	0.0278	0.7764	0.0493	0.0119	0.0004	35.55	2.72
05	6.5	172	188	0.4708	0.0288	0.7890	0.0457	0.0122	0.0005	36.43	2.93
06	6.1	61	345	0.3100	0.0318	0.3506	0.0291	0.0082	0.0003	35.27	4.05
07	10.3	39	347	0.4374	0.0301	0.6995	0.0730	0.0116	0.0007	37.91	3.66
08	12.6	148	241	0.5943	0.0296	1.4094	0.1028	0.0172	0.0009	34.35	2.77
09	7.1	51	223	0.4992	0.0279	0.8008	0.0612	0.0116	0.0006	32.22	2.77
10	20.6	34	329	0.6234	0.0247	1.7292	0.0985	0.0201	0.0009	35.43	2.43
11	3.7	24	173	0.3995	0.0456	0.4978	0.0470	0.0090	0.0005	32.32	4.25
12	4.4	50	242	0.3051	0.0242	0.3524	0.0242	0.0084	0.0004	36.36	3.55
13	10.6	97	380	0.4423	0.0299	0.7104	0.0651	0.0116	0.0007	37.61	3.58
14	12.4	36	308	0.5842	0.0345	1.0947	0.0722	0.0136	0.0006	28.27	2.31
15	9.8	241	193	0.5908	0.0405	1.3318	0.0861	0.0163	0.0008	33.13	2.98
16	31.1	353	442	0.6689	0.0282	2.0121	0.1069	0.0218	0.0008	30.40	1.99
17	10.5	180	283	0.5515	0.0276	1.0432	0.0624	0.0137	0.0006	32.17	2.41
18	6.0	143	333	0.3461	0.0257	0.3870	0.0317	0.0081	0.0003	32.51	2.97
19	7.5	194	283	0.4741	0.0349	0.6565	0.0440	0.0100	0.0004	29.85	2.74
20	16.5	207	473	0.5344	0.0271	0.9248	0.0586	0.0126	0.0004	31.17	2.23
21	8.6	199	417	0.4141	0.0287	0.5105	0.0363	0.0089	0.0003	30.93	2.64
22	17.0	188	454	0.5719	0.0406	1.2104	0.1591	0.0153	0.0014	33.45	4.04
23	12.0	294	507	0.4450	0.0317	0.5713	0.0787	0.0093	0.0006	29.87	3.12
24	13.8	96	356	0.5169	0.0274	0.9271	0.0776	0.0130	0.0007	34.14	2.89
25	15.8	97	387	0.5466	0.0337	1.1035	0.0896	0.0146	0.0009	34.90	3.30
26	4.3	378	286	0.2867	0.0202	0.2847	0.0201	0.0072	0.0002	32.35	2.70
27	4.5	326	294	0.2837	0.0235	0.2813	0.0201	0.0072	0.0002	32.47	3.08
28	6.9	526	304	0.4082	0.0202	0.5065	0.0279	0.0090	0.0003	31.55	2.23
29	23.7	77	206	0.7128	0.0162	3.3441	0.0845	0.0340	0.0006	35.29	1.63
30	6.7	58	394	0.3129	0.0216	0.3622	0.0237	0.0084	0.0003	35.91	3.00
31	19.1	287	536	0.4852	0.0176	0.9119	0.0314	0.0136	0.0003	39.26	2.22
32	20.4	383	1491	0.2781	0.0103	0.2709	0.0129	0.0071	0.0001	32.21	1.76
33	8.5	193	257	0.5284	0.0209	0.9381	0.0562	0.0129	0.0006	32.59	2.25
34	24.3	447	392	0.6123	0.0193	1.6741	0.0597	0.0198	0.0005	36.71	1.97
35	15.4	78	336	0.5794	0.0183	1.2930	0.0734	0.0162	0.0007	34.28	2.19
36	4.8	63	312	0.3179	0.0152	0.3359	0.0147	0.0077	0.0002	32.48	2.07
37	8.7	313	221	0.5238	0.0225	0.9794	0.0517	0.0136	0.0004	34.84	2.23
38	44.9	397	1286	0.4813	0.0139	0.8545	0.0377	0.0129	0.0003	37.50	1.97
39	22.1	315	560	0.5337	0.0156	1.0833	0.0546	0.0147	0.0005	36.62	2.09
40	7.1	385	431	0.3231	0.0186	0.3569	0.0230	0.0080	0.0003	33.62	2.52
41	6.3	173	212	0.4844	0.0235	0.7646	0.0455	0.0114	0.0004	33.06	2.30
42	4.5	124	217	0.3799	0.0215	0.4878	0.0235	0.0093	0.0003	34.78	2.54
43	14.8	211	277	0.6317	0.0294	1.5328	0.0663	0.0176	0.0006	29.83	2.01
44	8.3	210	373	0.4499	0.0293	0.5914	0.0847	0.0095	0.0007	30.21	3.07
45	6.3	151	217	0.4436	0.0256	0.6945	0.0556	0.0114	0.0006	36.53	3.10
46	5.7	143	175	0.4883	0.0225	0.8297	0.0412	0.0123	0.0006	35.20	2.62
47	7.9	198	241	0.5251	0.0242	0.9297	0.1015	0.0128	0.0009	32.85	3.06
48	8.9	67	236	0.5957	0.0280	1.4316	0.1241	0.0174	0.0012	34.62	3.08
49	4.0	77	229	0.3467	0.0223	0.3663	0.0368	0.0077	0.0003	30.69	2.57
50	4.0	76	291	0.2215	0.0199	0.2228	0.0166	0.0073	0.0002	36.61	3.72
51	14.5	210	144	0.7403	0.0309	3.1313	0.4363	0.0307	0.0036	25.00	3.22
52	12.9	99	192	0.7291	0.0407	2.2669	0.1769	0.0225	0.0015	20.43	1.89
53	4.4	251	256	0.3473	0.0293	0.3648	0.0303	0.0076	0.0004	30.47	3.17

6. Conclusions

Magmatic- and hydrothermal titanite are distinguished in the Beiya deposit, which occurs in the ore-related porphyry and mineralized skarn, respectively. Hydrothermal titanite is characterized by higher FeO, F, HFSEs, Nb/Ta and Lu/Hf, as well as lower TiO_2 and Th/U than magmatic titanite. It also displays a right-dipping REE pattern with lower LREE/HREE and more obvious negative Eu anomaly than its magmatic counterpart. REE characteristics of hydrothermal titanite indicate that the ore forming fluids might have been derived from relatively oxidized magma. Magmatic titanite from the porphyry has yielded a U–Pb age of 36.0 ± 5.9 Ma (coeval with the porphyry emplacement age), whilst hydrothermal titanite from the skarn has yielded a U–Pb age of 33.1 ± 1.0 Ma, representing the age of the retrograde skarn alteration. This robust titanite U–Pb age and the published molybdenite Re–Os age have altogether further constrained the Beiya mineralization to 33.1–34.1 Ma, suggesting that the mineralization was related to the post-magmatic hydrothermal activity in the Himalayan orogenic event.

Acknowledgments

This work was jointly funded by the National Natural Science Foundation of China (Nos. U1302233, 40830425, 40673045, 40873034), China Postdoctoral Science Foundation (No.2015M582457), the National Key Basic Research Program (Nos. 2015CB452604, 2009CB421006; Ministry of Science and Technology of the People's Republic of China), Higher School Specialized Research Fund for the Doctoral Program Funding Issue (No. 200805580031), and the Project Supported by Guangdong Province Universities and Colleges Pearl River Scholar Funded Scheme (No. 2011).

Table 4
LA–ICP–MS U–Pb isotope data for magmatic titanite from the Beiya deposit.

Sample no. W300	Pb	Th	U	Measured isotopic ratios			
	$\times 10^{-6}$			$^{207}Pb/^{206}Pb$	1σ	$^{206}Pb/^{238}U$	1σ
01	3.2	242	53	0.5923	0.0634	0.0166	0.0008
02	3.6	147	37	0.7455	0.0701	0.0269	0.0016
03	7.5	222	49	0.7965	0.0518	0.0386	0.0015
04	2.6	137	20	0.7757	0.3083	0.0312	0.0017
05	6.3	81.7	16	0.8783	0.0964	0.0934	0.0067
06	3.3	89.0	16	0.7384	0.2036	0.0555	0.0031
07	5.2	173	48	0.7463	0.0448	0.0283	0.0010
08	8.6	141	133	0.6954	0.0381	0.0192	0.0006
09	5.7	237	40	0.7113	0.0423	0.0389	0.0015
10	4.6	125	27	0.7930	0.0598	0.0485	0.0028
11	4.2	134	25	0.7523	0.0512	0.0457	0.0022
12	4.6	104	19	0.8089	0.0720	0.0630	0.0030
13	3.0	176	51	0.6580	0.0969	0.0171	0.0008
14	5.0	139	27	0.7768	0.0774	0.0487	0.0024
15	5.2	197	47	0.6677	0.0785	0.0314	0.0021
16	15.0	250	95	0.7125	0.0210	0.0420	0.0014
17	4.0	230	82	0.6030	0.0320	0.0180	0.0008
18	3.7	128	18	0.7923	0.0337	0.0512	0.0013
19	4.2	163	25	0.7722	0.0298	0.0444	0.0010
20	13.2	175	28	0.8036	0.0263	0.1194	0.0037
21	3.0	117	23	0.7897	0.0506	0.0356	0.0017
22	4.0	187	51	0.6961	0.0329	0.0219	0.0008
23	2.8	206	50	0.6141	0.0348	0.0163	0.0006
24	2.7	196	50	0.5810	0.0344	0.0161	0.0005
25	5.1	71.4	14	0.7867	0.0438	0.0947	0.0030
26	2.6	199	48	0.6267	0.0332	0.0150	0.0004
27	2.9	235	64	0.5538	0.0306	0.0142	0.0004
28	2.7	203	41	0.5734	0.0813	0.0186	0.0013
29	4.8	207	47	0.8097	0.0876	0.0257	0.0017

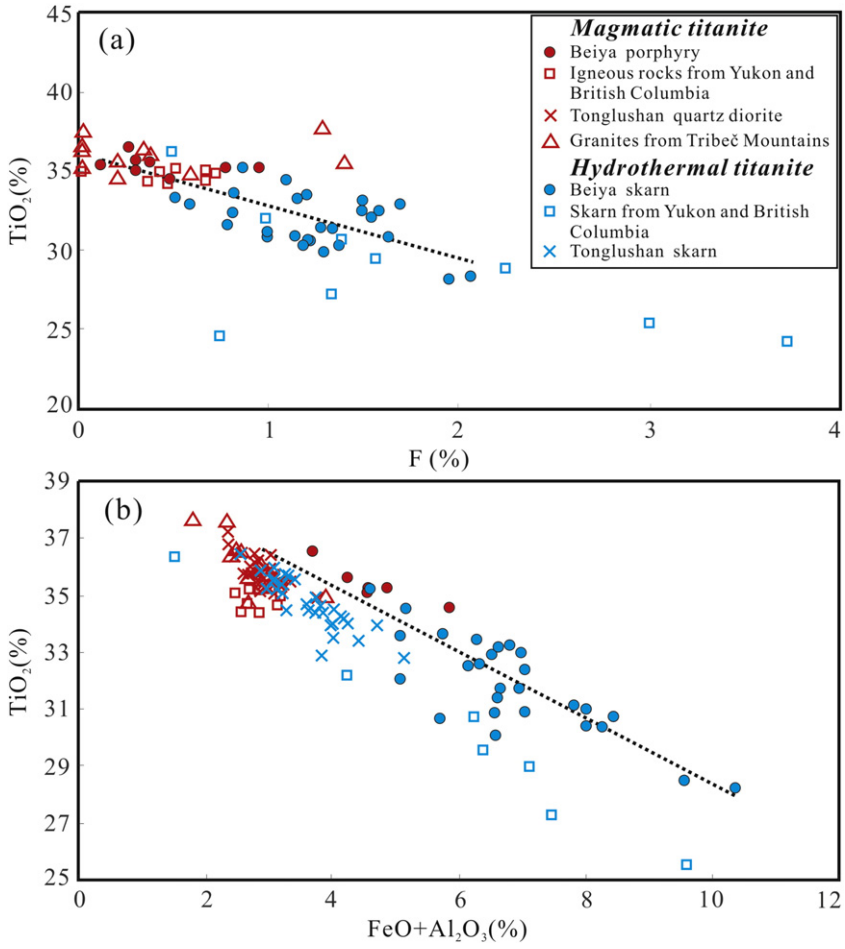

Fig. 7. Binary plots of (a) F versus TiO_2 and (b) FeO + Al_2O_3 versus TiO_2 in magmatic and hydrothermal titanites. (The values of other magmatic and hydrothermal titanites are from Broska et al., 2007; Li et al., 2010; Che et al., 2013.)

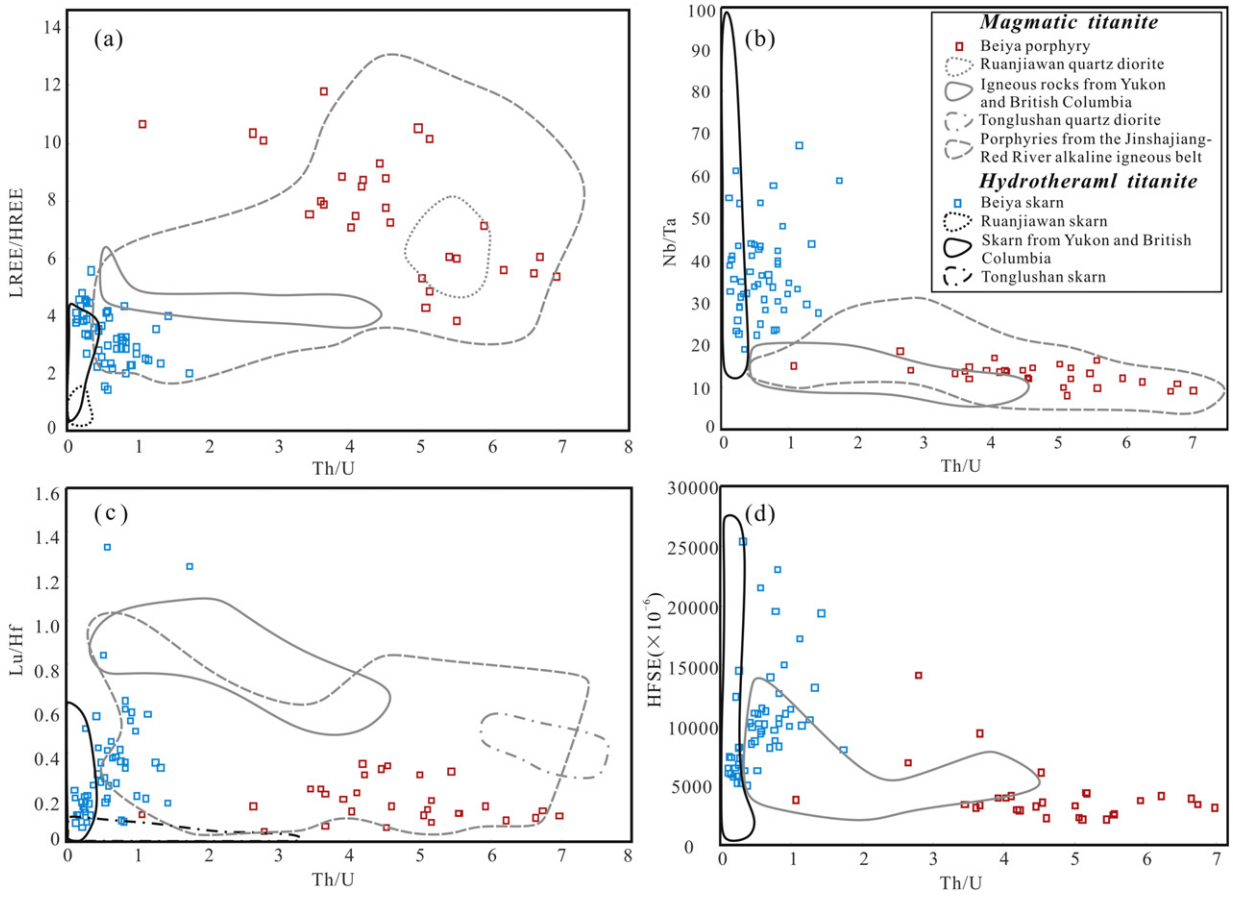

Fig. 8. Plots of Th/U versus (a) LREE/HREE, (b) Nb/Ta, (c) Lu/Hf, and (d) HFSE showing distinct geochemical characteristics of magmatic and hydrothermal titanites. (The values of other magmatic and hydrothermal titanites are from Li et al., 2010; Che et al., 2013; Deng et al., 2015a, b; Xu et al., 2015.)

References

Aleinikoff, J.N., Wintsch, R.P., Fanning, C.M., Dorais, M.J., 2002. U–Pb geochronology of zircon and polygenetic titanite from the Glastonbury Complex, Connecticut, USA: an integrated SEM, EMPA, TIMS, and SHRIMP study. Chem. Geol. 188 (1), 125–147.

Bonamici, C.E., Fanning, C.M., Kozdon, R., Fournelle, J.H., Valley, J.W., 2015. Combined oxygen-isotope and U–Pb zoning studies of titanite: new criteria for age preservation. Chem. Geol. 398, 70–84.

Broska, I., Harlov, D., Tropper, P., Siman, P., 2007. Formation of magmatic titanite and titanite–ilmenite phase relations during granite alteration in the Tribeč Mountains, Western Carpathians, Slovakia. Lithos 95, 58–71.

Cao, M.J., Qin, K.Z., Li, G.M., Evans, N.J., Jin, L.Y., 2015. In situ LA-(MC)-ICP-MS trace element and Nd isotopic compositions and genesis of polygenetic titanite from the Baogutu reduced porphyry Cu deposit, Western Junggar, NW China. Ore Geol. Rev. 65, 940–954.

Cempírek, J., Houzar, S., Novák, M., 2008. Complexly zoned niobian titanite from hedenbergite skarn at Písek, Czech Republic, constrained by substitutions $Al(Nb,Ta)Ti_{-2}$, $Al(F,OH)(TiO)_{-1}$ and $SnTi_{-1}$. Mineral. Mag. 72 (6), 1293–1305.

Che, X.D., Linnen, R.L., Wang, R.C., Groat, L.A., Brand, A.A., 2013. Distribution of trace and rare earth elements in titanite from tungsten and molybdenum deposits in Yukon and British Columbia, Canada. Can. Mineral. 51 (3), 415–438.

Chelle-Michou, C., Chiaradia, M., Selby, D., Ovtcharova, M., Spikings, R.A., 2015. High-resolution geochronology of the Coroccohuayco porphyry–skarn deposit, Peru: a rapid product of the Incaic orogeny. Econ. Geol. 110, 423–443.

Chiaradia, M., Vallance, J., Fontbote, L., Stein, H., Schaltegger, U., Coder, J., Richards, J., Villeneve, M., Gendall, I., 2009. U–Pb, Re–Os, and $^{40}Ar/^{39}Ar$ geochronology of the Nambija Au-skarn and Pangui porphyry Cu deposits, Ecuador: implications for the Jurassic metallogenic belt of the Northern Andes. Mineral. Deposita 44 (4), 371–387.

Chiaradia, M., Schaltegger, U., Spikings, R., Wotzlaw, J.F., Ovtcharova, M., 2013. How accurately can we date the duration of magmatic-hydrothermal events in porphyry systems? — an invited paper. Econ. Geol. 108, 565–584.

Corfu, F., Grunsky, E.C., 1987. Igneous and tectonic evolution of the Batchawana greenstone belt, Superior Province: a U–Pb zircon and titanite study. J. Geol. 95 (1), 87–105.

Corfu, F., Heaman, L.M., Rogers, G., 1994. Polymetamorphic evolution of the Lewisian complex, NW Scotland, as recorded by U–Pb isotopic compositions of zircon, titanite and rutile. Contrib. Mineral. Petrol. 117 (3), 215–228.

Deng, X.D., Li, J.W., Zhou, M.F., Zhao, X.F., Yan, D.R., 2015a. In-situ LA-ICPMS trace elements and U–Pb analysis of titanite from the Mesozoic Ruanjiawan W–Cu–Mo skarn deposit, Daye district, China. Ore Geol. Rev. 65, 990–1004.

Deng, J., Qang, Q.F., Li, G.J., Hou, Z.Q., Jiang, C.Z., Danyushevsky, L., 2015b. Geology and genesis of giant Beiya porphyry–skarn gold deposit, northwestern Yangtze Block, China. Ore Geol. Rev. 70, 457–485.

Esssex, R.M., Gromet, L.P., 2000. U–Pb dating of prograde and retrograde titanite growth during the Scandian orogeny. Geology 28 (5), 419–422.

Fallourd, S., Poujol, M., Boulvais, P., Paquette, J.L., Blanquat, M.S., Remy, P., 2014. In situ LA-ICP-MS U–Pb titanite dating of Na–Ca metasomatism in orogenic belts: the North Pyrenean example. Int. J. Earth Sci. 103 (3), 667–682.

Frost, B.R., Chamberlain, K.R., Schumacher, J.C., 2000. Sphene (titanite): phase relations and role as a geochronometer. Chem. Geol. 172 (1), 131–148.

Fu, Y., Sun, X.M., Lin, H., Zhou, H.Y., Li, X., Ouyang, X.Q., Jiang, L.Y., Shi, G.Y., Liang, Y.H., 2015. Geochronology of the giant Beiya gold-polymetallic deposit in Yunnan Province, Southwest China and its relationship with the petrogenesis of alkaline porphyry. Ore Geol. Rev. 71, 138–149.

Gao, X.Y., Zheng, Y.F., Chen, Y.X., Guo, J.L., 2012. Geochemical and U–Pb age constraints on the occurrence of polygenetic titanites in UHP metagranite in the Dabie orogen. Lithos 136-139, 93–108.

Gregory, C.J., McFarlane, C.R.M., Hermann, J., Rubatto, D., 2009. Tracing the evolution of calc-alkaline magmas: in-situ Sm–Nd isotope studies of accessory minerals in the Bergell Igneous Complex, Italy. Chem. Geol. 260 (1–2), 73–86.

Guo, Y.S., Zeng, P.S., Yang, W.G., Zhang, W.H., 2005. Geological characteristics and metallogenic types of Beiya gold-polymetallic deposit, in Yunnan. Eng. Sci. 7, 218–223 (in Chinese with English abstract).

Guo, J.L., Gao, S., Wu, Y.B., Hu, Z.C., Xu, W.L., Zong, K.Q., Liu, Y.S., Yuan, H.L., 2014. Titanite evidence for Triassic thickened lower crust along southeastern margin of North China Craton. Lithos 206-207, 277–288.

Hayden, L.A., Watson, E.B., Wark, D.A., 2008. A thermobarometer for sphene (titanite). Contrib. Mineral. Petrol. 155 (4), 529–540.

He, W.Y., 2014. The Beiya Giant Gold-polymetallic Deposit: Magmatism and Metallogenic Model (Ph.D. thesis) China University of Geosciences (Beijing) Beijing. (in Chinese with English abstract).

He, W.Y., Yu, X.H., Mo, X.X., He, Z.H., Li, Y., Huang, X.K., Su, G.S., 2012. Genetic type and the relationship between alkali-rich intrusion and mineralization of Beiya gold-polymetallic ore field, western Yunnan Province, China. Acta Petrol. Sin. 28, 1401–1412 (in Chinese with English abstract).

He, Z.H., Zhou, Y.M., He, W.Y., Su, G.S., Li, W.H., Yang, S.W., 2013. Genetic types and metallogenic regularity of Beiya superlarge gold-polymetallic deposit, northwestern Yunnan. Mineral Deposits 32, 244–258 (in Chinese with English abstract).

He, W.Y., Mo, X.X., He, Z.H., White, N.C., Chen, J.B., Yang, K.H., Wang, R., Yu, X.H., Dong, G.C., Huang, X.F., 2015. The geology and mineralogy of the Beiya skarn gold deposit in Yunnan, Southwest China. Econ. Geol. 110, 1625–1641.
Hermann, J., Spandler, C., Hack, A., Korsakov, A.V., 2006. Aqueous fluids and hydrous melts in high-pressure and ultra-high pressure rocks: implications for element transfer in subduction zones. Lithos 92, 399–417.
Horie, K., Hidaka, H., Gauthier-Lafaye, F., 2008. Elemental distribution in apatite, titanite and zircon during hydrothermal alteration: durability of immobilization mineral phases for actinides. Phys. Chem. Earth 33, 962–968.
Hou, Z.Q., Zhong, D.L., Deng, W.M., 2004. A tectonic model for porphyry copper–molybdenum–gold metallogenic belt on the eastern margin of the Qinghai–Tibet Plateau. Geol. China 31, 1–14 (in Chinese with English abstract).
Ismail, R., Ciobanu, C.L., Cook, N.J., Teale, G.S., Giles, D., Mumm, A.S., Wade, B., 2014. Rare earths and other trace elements in minerals from skarn assemblages, Hillside iron oxide–copper–gold deposit, Yorke Peninsula, South Australia. Lithos 184-187, 456–477.
Kohn, M.J., Corrie, S.L., 2011. Preserved Zr-temperatures and U–Pb ages in high-grade metamorphic titanite: evidence for a static hot channel in the Himalayan orogen. Earth Planet. Sci. Lett. 311 (1–2), 136–143.
Li, J.W., Deng, X.D., Zhou, M.F., Liu, Y.S., Zhao, X.F., Guo, J.L., 2010. Laser ablation ICP-MS titanite U–Th–Pb dating of hydrothermal ore deposits: a case study of the Tonglushan Cu–Fe–Au skarn deposit, SE Hubei Province, China. Chem. Geol. 270, 56–67.
Li, W.C., Wang, J.H., He, Z.H., Dou, S., 2016. Formation of Au-polymetallic ore deposits in alkaline porphyries at Beiya, Yunnan, Southwest China. Ore Geol. Rev. 73, 241–252.
Liu, Y.S., Gao, S., Hu, Z.C., Gao, C.G., Zong, K.Q., Wang, D.B., 2010. Continental and oceanic crust recycling-induced melt-peridotite interactions in the Trans-North China orogen: U–Pb dating, Hf isotopes and trace elements in zircons from mantle xenoliths. J. Petrol. 51, 537–571.
Liu, B., Liu, H., Zhang, C.Q., Mao, Z.H., Zhou, Y.M., Huang, H., He, Z.H., Su, G.S., 2015. Geochemistry and geochronology of porphyries from the Beiya gold-polymetallic orefield, western Yunnan, China. Ore Geol. Rev. 69, 360–379.
Lu, Y.J., Kerrich, R., Cawood, P.A., McCuaig, T.C., Hart, C.J.R., Li, Z.X., Hou, Z.Q., Bagas, L., 2012. Zircon SHRIMP U–Pb geochronology of potassic felsic intrusions in western Yunnan, SW China: constraints on the relationship of magmatism to the Jinsha suture. Gondwana Res. 22, 737–747.
Lu, Y.J., Kerrich, R., Kemp, A.I.S., McCuaig, T.C., Hou, Z.Q., Hart, C.J.R., Li, Z.X., Cawood, P.A., Bagas, L., Yang, Z.M., Cliff, J., Belousova, E.A., Jourdan, F., Evans, N.J., 2013a. Intracontinental Eocene–Oligocene porphyry Cu mineral systems of Yunnan, western Yangtze Craton, China: compositional characteristics, sources, and implications for continental collision metallogeny. Econ. Geol. 108, 1541–1576.
Lu, Y.J., Kerrich, R., McCuaig, T.C., Li, Z.X., Hart, C.J.R., Cawood, P.A., Hou, Z.Q., Bagas, L., Cliff, J., Belousova, E.A., Tang, S.H., 2013b. Geochemical, Sr–Nd–Pb, and zircon Hf–O isotopic compositions of Eocene–Oligocene shoshonitic and potassic adakite-like felsic intrusions in western Yunnan, SW China: petrogenesis and tectonic implications. J. Petrol. 54, 1309–1348.
Ludwig, K.R., 2003. User's Manual for Isoplot 3.0: a Geochronological Toolkit for Microsoft Excel. Special Publication 4. Berkeley Geochronology Center, pp. 1–70.
Mazdab, F.K., 2009. Characterization of flux-grown trace-element-doped titanite using the high-mass-resolution ion microprobe (SHRIMP-RG). Can. Mineral. 47 (4), 813–831.
Morad, S., El-Ghali, M.A.K., Caja, M.A., Al-Ramadan, K., Mansurbeg, H., 2009. Hydrothermal alteration of magmatic titanite: evidence from Proterozoic granitic rocks, Southeastern Sweden. Can. Mineral. 47 (4), 801–811.
Olin, P.H., Wolff, J.A., 2012. Partitioning of rare earth and high field strength elements between titanite and phonolitic liquid. Lithos 128-131, 46–54.
Pan, Y., Fleet, M.E., MacRae, N.D., 1993. Late alteration in titanite ($CaTiSiO_5$): redistribution and remobilization of rare earth elements and implications for U/Pb and Th/Pb geochronology and nuclear waste disposal. Geochim. Cosmochim. Acta 57 (2), 355–367.
Sepahi, A.A., Shahbazi, H., Siebel, W., Ranin, A., 2014. Geochronology of plutonic rocks from the Sanandaj-Sirjan zone, Iran and new zircon and titanite U–Th–Pb ages for granitoids from the Marivan pluton. Geochronometria 41 (3), 207–215.
Smith, M.P., Storey, C.D., Jeffries, T.E., Ryan, C., 2009. In situ U–Pb and trace element analysis of accessory minerals in the Kiruna District, Norrbotten, Sweden: new constraints on the timing and origin of mineralization. J. Petrol. 50 (11), 2063–2094.
Stacey, J.S., Kramers, J.D., 1975. Approximation of terrestrial lead isotope evolution by a two-stage model. Earth Planet. Sci. Lett. 26, 207–221.
Stern, R.A., 1997. The GSC sensitive high resolution ion microprobe (SHRIMP): analytical techniques of zircon U–Th–Pb age determinations and performance evaluation. Radiogenic age and isotopic studies: report 10. Geol. Surv. Can. Curr. Res. 1997-F, 1–31.
Storey, C.D., Jeffries, T.E., Smith, M., 2006. Common lead-corrected laser ablation ICP–MS U–Pb systematics and geochronology of titanite. Chem. Geol. 227, 37–52.
Storey, C.D., Smith, M.P., Jeffries, T.E., 2007. In situ LA-ICP-MS U–Pb dating of metavolcanics of Norrbotten, Sweden: records of extended geological histories in complex titanite grains. Chem. Geol. 240 (1–2), 163–181.
Sun, S.S., McDonough, W.F., 1989. Chemical and isotopic systematics of oceanic basalts: implications for mantle composition and processes. Geol. Soc. Lond. Spec. Publ. 42, 313–345.
Sun, J.F., Yang, J.H., Wu, F.Y., Li, X.H., Yang, Y.H., Xie, L.W., Wilde, S.A., 2010. Magma mixing controlling the origin of the Early Cretaceous Fangshan granitic pluton, North China Craton: in situ U–Pb age and Sr-, Nd-, Hf- and O-isotope evidence. Lithos 120, 421–438.
Sun, J.F., Yang, J.H., Wu, F.Y., Xie, L.W., Yang, Y.H., Liu, Z.C., Li, X.H., 2012. In situ U–Pb dating of titanite by LA-ICPMS. Chin. Sci. Bull. 57 (20), 2506–2516.
Tiepolo, M., Oberti, R., Vannucci, R., 2002. Trace-element incorporation in titanite: constraints from experimentally determined solid/liquid partition coefficients. Chem. Geol. 191, 105–119.
Wang, J.H., Yin, A., Harrison, T.M., Grove, M., Zhang, Y.Q., Xie, G.H., 2001. A tectonic model for Cenozoic igneous activities in the eastern Indo–Asian collision zone. Earth Planet. Sci. Lett. 188, 123–133.
Xiao, X.N., Yu, X.H., Mo, X.X., Yang, G.L., Li, Y., Huang, X.K., 2009. Geochemistry, zircon SHRIMP U–Pb dating and origin of alkali-rich porphyries in Beiya area, north Erhai Lake, western Yunnan, China. Geol. Bull. Chin. 28, 1786–1803 (in Chinese with English abstract).
Xie, L., Wang, R.C., Chen, J., Zhu, J.C., 2010. Mineralogical evidence for magmatic and hydrothermal processes in the Qitianling oxidized tin-bearing granite (Hunan, South China): EMP and (MC)-LA-ICPMS investigations of three types of titanite. Chem. Geol. 276, 53–68.
Xu, X.W., Cai, X.P., Song, B.C., Zhang, B.L., Ying, H.L., Xiao, Q.B., Wang, J., 2006a. Petrologic, chronological and geochemistry characteristics and formation mechanism of alkaline porphyries in the Beiya gold district, western Yunnan. Acta Petrol. Sin. 22, 631–643 (in Chinese with English abstract).
Xu, S.M., Mo, X.X., Zeng, P.S., Zhang, W.H., Zhao, H.B., Zhao, H.D., 2006b. Characteristics and origin of alkali-rich porphyries from Beiya in Western Yunnan. Geoscience 20, 527–535 (in Chinese with English abstract).
Xu, X.W., Cai, X.P., Zhang, B.L., Liang, G.H., Du, S.J., Wang, J., 2007a. Genetic types and framework model of Beiya gold ore district in western Yunnan. Mineral Deposits 26, 249–264 (in Chinese with English abstract).
Xu, X.W., Cai, X.P., Xiao, Q.B., Peters, S.G., 2007b. Porphyry Cu–Au and associated polymetallic Fe–Cu–Au deposits in the Beiya Area, western Yunnan Province, south China. Ore Geol. Rev. 31, 224–246.
Xu, L., Bi, X.W., H, R.Z., Tang, Y.Y., Wang, X.S., Xu, Y., 2015. LA-ICP-MS mineral chemistry of titanite and the geological implications for exploration of porphyry Cu deposits in the Jinshajiang–Red River alkaline igneous belt, SW China. Mineral. Petrol. 109 (2), 181–200.
Xue, C.D., Hou, Z.Q., Liu, X., Yang, Z.M., Liu, Y.Q., Hao, B.W., 2008. Petrogenesis and metallogenesis of the Beiya gold-polymetallic ore district, northwestern Yunnan province, China: responses to the Indo-Asian collisional processes. Acta Petrol. Sin. 24, 457–472 (in Chinese with English abstract).
Zhu, Q.Q., Xie, G.Q., Jiang, Z.S., Sun, J.F., Li, W., 2014. Characteristics and in situ U–Pb dating of hydrothermal titanite by LA-ICPMS of the Jingshandian iron skarn deposit, Hubei Province. Acta Petrol. Sin. 30 (5), 1322–1338 (in Chinese with English abstract).